TÉCNICO LISBOA

Entangled Photon Pair Source for Free-Space Quantum Communication

Gonçalo Lobato Baptista Teixeira

Thesis to obtain the Master of Science Degree in

Engineering Physics

Supervisors: Prof. João Carlos Carvalho de Sá Seixas
Prof. Yasser Rashid Revez Omar

Examination Committee

Chairperson: Prof. Pedro Miguel Félix Brogueira
Supervisor: Prof. João Carlos Carvalho de Sá Seixas
Member of the Committee: Prof. Gonçalo Nuno Marmelo Foito Figueira

December 2022

Declaration

I declare that this document is an original work of my own authorship and that it fulfills all the requirements of the Code of Conduct and Good Practices of the Universidade de Lisboa.

Acknowledgments

I would like to acknowledge my dissertation supervisors, Professors Yasser Omar and João Seixas, for their insight and support throughout the project.

I would like to extend a special thank you to Dr. Emmanuel Zambrini Cruzeiro for his supervision, and my colleagues in the laboratory, Pedro Mendes and José Senart, for all their assistance and friendship during my thesis work. I have learned a lot in the Quantum Photonics Laboratory (QuLab) this year, and their guidance and motivation helped me move forward and overcome the obstacles I faced. I am very grateful for their help in this final phase of my studies.

I want to thank my parents for their encouragement and care over all throughout my life, pushing me to achieve my goals and believing in me. To my brother, I want to thank his support and companionship. I would also like to thank my grandparents, aunt, uncle and cousin for their understanding and support throughout the years.

I am grateful to my ”friend-at-arms”, Luísa, the first person I met at the university. Since the beginning of my studies, we have been inseparable. Together we overcame many difficulties. We were there for each other in the most challenging moments, and at the end of the day, we always shared a big laugh.

Last but not least, to all the special people in my life who helped me grow and were always there when I need the most. Thank you.

To each and every one of you – Thank you.

Resumo

Informação é um dos recursos mais valiosos do mundo e a informação quântica visa trazer um novo paradigma. Um dos ingredientes essenciais para as tecnologias de fotónica quântica, em particular comunicações quânticas seguras, são fontes de pares de fotões entrelaçados. O entrelaçamento quântico é uma propriedade particular dos sistemas quânticos que permite a implementação de comunicações seguras que de outra forma seriam impossíveis com informação clássica. Uma fonte de pares de fotões entrelaçados pode ser usada adicionalmente como Heralded Single Photon Source (HSPS) para experiências ópticas de Quantum Key Distribution (QKD). Nesta tese, desenvolvemos uma fonte de pares de fotões para telecomunicações em espaço livre capaz de produzir estados quânticos de alta qualidade. Para gerar entrelaçamento quântico, usámos um processo óptico não linear chamado Spontaneous Parametric Down Conversion (SPDC), que gera pares de fotões correlacionados. Caracterizamos estes pares usando um interferômetro Hong-Ou-Mandel (HOM) para medir e compensar o seu atraso temporal. Também usámos o Bell State Analyzer para medir a qualidade do entrelaçamento. Em adição, desenvolvemos um design preliminar para um emissor de estados quânticos ótico miniaturizado que serve como base para o design do primeiro nano satélite português para comunicações quânticas.

Palavras Chave

Entrelaçamento Quântico; Ótica Não Linear; Pares de Fotões; Comunicações Quânticas; Nano satélite

Abstract

Information is one of the world's most valuable resources, and quantum information aims to bring this matter to a new paradigm. One of the essential ingredients for photonic quantum technologies, namely secure quantum communications, are entangled photon pair sources. Entanglement is a particular property of quantum systems that allows the implementation of secure communications that would be impossible using classical information. An entangled photon pair source may additionally be used as a Heralded Single Photon Source (HSPS) for optical implementations of Quantum Key Distribution (QKD). In this thesis, we developed a photon pair source for free-space telecommunications, capable of producing high-quality quantum states. To produce quantum entanglement, we used a nonlinear optical process called Spontaneous Parametric Down Conversion (SPDC), which generates correlated pairs of photons. We characterize the photon pairs using a Hong-Ou-Mandel (HOM) interferometer to measure and compensate for their temporal delay. We employed a Bell State Analyzer to measure the quality of entanglement attained. Additionally, we developed a preliminary design for a miniaturized quantum state emitter optical payload, which serves as a basis for the design of the first Portuguese nanosatellite for quantum communications.

Keywords

Entanglement; Nonlinear Optics; Photon Pairs; Quantum Communication; Nanosatellite.

Contents

List of Figures

List of Tables

Acronyms

BER	Bit Error Rate
BS	Beam Splitter
CCD	Charge-Coupled Device
DM	Dichroic Mirror
EOAM	Electro-Optic Amplitude Modulator
EOM	Electro-Optic Modulator
EOPM	Electro-Optic Phase Modulator
FPGA	Field Programmable Gate Array
FWHM	Full Width at Half Maximum
HSPS	Heralded Single Photon Source
HOM	Hong-Ou-Mandel
HSPS	Heralded Single Photon Source
HWP	Half Wave Plate
IR	Infra Red
LEO	Low Earth Orbit
PBS	Polarization Beam Splitter
PC	Polarization Controller
PF	Passive Filter
PM	Phase Matching
POVM	Positive Operator-Valued Measure
PP	Periodically Poled
PPKTP	Periodically Poled Potassium Titanyl Phosphate
PSD	Positive Semi-Definite

QKD	Quantum Key Distribution
QPM	Quasi Phase Matching
QWP	Quarter Wave Plate
SatQKD	Satellite Quantum Key Distribution
SFWM	Spontaneous Four Wave Mixing
SPCM	Single Photon Counting Module
SPDC	Spontaneous Parametric Down Conversion
TCSPC	Time Correlated Single Photon Counting
UV	Ultra Violet
WCP	Weak Coherent Pulse
WFG	Wave Function Generator

1

Introduction

Contents

The 20th century brought a great revolution in physics with the birth of new fields and concepts like quantum mechanics. This drastic change in perspective in our way of imagining the world made us go from studying the phenomena that we observe on a daily basis to trying to describe what happens on microscopic scales, down to individual particles.

In 1935, Albert Einstein, Boris Podolsky and Nathan Rosen proposed that the wave function (fundamental concept of quantum mechanics) does not provide a complete description of physical reality [2]. Their reasoning was that entangled particles disrupt an already established concept of physics, that information cannot travel faster than the speed of light. They conclude that adding "hidden variables" is necessary for a complete theory. However, later in 1964, John Bell developed a new theorem that introduces a numerical inequality if the hidden variables exist [3]. If the inequality is violated, the hidden variables theory does not entirely describe quantum mechanics.

Bell's theorem was only verified experimentally in 1982 by Alain Aspect, Phillippe Grangier, and Gérard Roger [4]. They measured Bell quantity of 2.70 ± 0.05 which is 14 standard deviations greater than the inequality limit (≤ 2). The experiment was a considerable challenge for the technology available at that time. It took three years and increasingly more complex setups to finally verify the Bell's inequality. The experiment is based on the polarization of light particles - photons, generated by a nonlinear optical process (Radiative Cascade in Calcium atoms) excited by a krypton laser. Since then, quantum optics has not only evolved more precise and complex Bell violation experiments with very small setups but also evolved into new kinds of quantum technologies applications.

The emerging field of quantum technologies is very promising. Quantum technologies use quantum information instead, and its functionality is based on unique principles of quantum mechanics like quantum superposition, tunnelling and entanglement. These phenomena give an all-new perspective on how we process and transmit information, which was impossible to achieve with classical information. Over the years, quantum technologies have seen a significant evolution, with tremendous progress in the areas of quantum computing [5, 6], quantum sensing [7], and quantum communications [8].

Quantum communication is the science of communicating private messages encoded in quantum states. The primary motivations are that quantum information – called qubits in their simplest form (two-level system) – enables specific tasks to be performed more efficiently than their classical counterpart. One example is Quantum Key Distribution (QKD) protocols [9, 10] that allow secure information in a way that cannot be achieved with nowadays technology. Quantum measurement has an active action on the state where it is performed, and quantum cryptography takes that advantage to create QKD protocols that detect an eavesdropper in communication. Another fascinating feature of quantum information is the process of quantum teleportation, which is based on using entangled particles to transfer information from a quantum state at one location to another quantum state some distance away [11, 12].

This year, Alan Aspect, John F. Clauser and Anton Zeilinger were awarded the Nobel prize in physics

for their work in experiments with entangled photons, establishing the violation of Bell's inequalities. This pioneering work in quantum information science used light particles as qubits. Quantum light offers many degrees of freedom to encode quantum information, like wavelength, polarization, path, orbital angular momentum, and time. Although photons are very easy to produce, specific states of light must be manufactured in the lab, such as entangled and squeezed states, which enable quantum advantage in different applications. For example, most experiments use a single particle/photon gun or an entangled two-photon source in quantum communications. This is because standard QKD protocols are formulated using single quanta or Bell pairs.

1.1 State of the Art

Correlated photon pairs are widely used in developing quantum technologies and demonstrating particular quantum phenomena [13]. They are commonly used in quantum communications [14, 15], quantum cryptography [16], quantum computing [17, 18] and many other uses [19–21]. Quantum phenomena are well studied using photons since they are very easy to produce and much less expensive than other alternatives.

Photon pair sources can be based on nonlinear processes where high-energy laser photons degenerate into two or more lower-energy correlated or entangled photons. There are processes of different orders, with different numbers of photons in input and output. These probabilistic sources are based on spontaneous nonlinear optical processes, which generate high-quality outputs and are more straightforward to implement. Such processes occur in passive nonlinear optical media such as crystals [22] or optical fibres [23]. These sources are relatively easy to operate compared to other sources with the capability of high-fidelity entanglement generation [24]. However, the efficiency of the photon pair production is limited by the nonlinear coefficient and the crystals' length to conserve the light's momentum during the process [25].

At present, quantum communications and quantum cryptography are taking a giant leap, with much research applied to overcome several challenges and with QKD systems already commercially available. These systems currently rely primarily on attenuated laser pulses rather than single photons. This means that a laser beam is attenuated until we have a train of single photons on average. However, this method differs from a single photon source due to the probabilistic nature of photons. The photon statistics follow a Poissonian distribution [26]. To be specific, there is always a trade-off between the probability of emitting a vacuum state ($n = 0$) or multi-photon states ($n > 1$). Operating the source at low power reduces the probability of multi-photon emission. QKD is not ready to be widely adopted since it faces crucial challenges such as secret key rate, distance, size, cost, and practical security [27]. If the number of photons that can be sent in communication is small, we will not have a secret key of the size

needed to encrypt messages. The range of communication is limited by the field of view (free-space communication) or by optical fibers, which limit the overall distance.

In recent years, Satellite Quantum Key Distribution (SatQKD) has overcome some limitations. The Chinese space mission, Micius [28], launched in 2016, has successfully demonstrated various quantum communication protocols in space [16, 29, 30]. These groundbreaking results have started an international space race, and now other countries and space agencies are designing SatQKD missions, including Japan [31], Canada [32], Austria/France [33] and more. The aim is to establish the first global quantum communication network but also to develop new architectures to merge other areas of quantum technologies, such as computing and sensing. These projects focus primarily on Low Earth Orbit (LEO) satellites, but there is a growing interest for higher earth orbits as well [34]. However, the Micius satellite is hefty and expensive, so there is an increasing interest in smaller and cheaper satellites for the possibility of establishing quantum communication services using a constellation [35].

A global quantum network would allow a new era for the secure exchange of information. However, it is difficult to predict the future of quantum technologies. It seems probable that quantum information will be transmitted in quantum states of light, and at some level, information processing will be performed in those states. Therefore, developments in quantum photonics are necessary to exploit the full potential of such technologies.

1.2 Thesis Overview

This thesis is a project on the experimental study of entangled particles and developing possible uses for quantum technologies, particularly quantum communications. The project aims at building an optical setup of a source that generates entangled photon pairs. Since it takes advantage of nonlinear optical phenomena to produce the pairs, the source is probabilistic. In addition, with this type of source is possible to build an Heralded Single Photon Source (HSPS) which can be used to implement a QKD protocol to transmit an encrypted key that any classic computer can breach. This will serve as a proof-of-principle setup for a quantum payload for space-earth communications over a distance of several kilometres that is included in the project QuantSat-PT.

The thesis is composed of five main chapters. The chapter 2 briefly describes the mathematical interpretation of quantum information and the properties of entangled states. (chapters 2 and 3). The chapter 3 is theoretical as well, but instead describes the physics of the nonlinear process that generates the photon pairs. Then in chapters 4 and 5, we describe the optical setup and the characterization of photon pairs. The characterization includes a study of the spatial profile, temporal profile and a test of the CHSH inequality. Finally, the chapter 6 is a plan of using the setup built in an application of QKD as a future demonstration for the project QuantSat-PT.

2

Finite-Dimensional Quantum Mechanics

Contents

Most seminal works and proof-of-principle demonstrations in quantum information use finite-dimensional quantum mechanics. In this work, we restrict to that case. This chapter aims to review the fundamental concepts of quantum information in an abstract mathematical way to understand more precisely the concept of quantum states and quantum entanglement.

2.1 Quantum Bits

The bit is the fundamental concept of classical digital information and computation. Quantum information is built upon an analogous concept, the quantum bit or qubit for short. As a classic bit, the qubit can have two possible states of either $|0\rangle$ or $|1\rangle$. However, the difference to the classical bit is that it can be in other states and be in a form superposition of those states (2.1).

$$|\psi\rangle = \alpha|0\rangle + \beta|1\rangle \tag{2.1}$$

α and β are complex numbers that describe the qubit's quantum state. The state (wavefunction) of a qubit is a vector in a two-dimensional complex vector space, where $|0\rangle$ and $|1\rangle$ form an orthonormal basis for this vector space. The quantum mechanical description of the state is an asymptotic one, which assumes that we have performed an infinite amount of measurements on it, to determine the coefficients α and β. In reality, in each run of the experiment, one only retrieves restricted information about the quantum state. Therefore, to determine the wavefunction, one must accumulate statistics.

A measurement of a qubit will either yield the result 0, with probability $|\alpha|^2$, or the result 1, with probability $|\beta|^2$. Since the probabilities must sum to one, $|\alpha|^2 + |\beta|^2 = 1$, the qubit's state $|\psi\rangle$ is a unit vector in the state space, which is described as $\langle\psi|\psi\rangle = 1$. This condition is known as the normalization condition for state vectors, and guarantees that the computed probabilities are indeed valid probabilities.

Suppose now that we have two qubits. In this kind of system, there are four possible measurement outcomes $|00\rangle$, $|01\rangle$, $|10\rangle$ and $|11\rangle$, where the first digit represents the state of the qubit one, and the second digit represents the qubit two. These outcomes form an orthonormal basis in a four-dimensional complex vector space. The quantum system of the two qubits involves the superposition of the four basis states, each associated with a complex coefficient. An important example of a two-qubit state is the Bell state $|\Psi^+\rangle$, also known as EPR pair [2, 5],

$$|\Psi^+\rangle = \frac{|01\rangle + |10\rangle}{\sqrt{2}} \tag{2.2}$$

This Bell state has a special property. Upon measuring the first qubit, the measurement of the second qubit will always give the opposite result, meaning the measurement outcomes are anticorrelated. For example, if the measurement on the first qubit gives the result 0 with probability $1/2$, the global state

becomes $|01\rangle$, and if the measurement on the first qubit gives the result 1 with probability $1/2$, the state becomes $|10\rangle$. This state is responsible for most applications in quantum information, and is the key concept for example behind quantum teleportation [11, 12], and device-independent quantum communication protocols [36].

2.2 The Density Matrix

The density matrix is another way to describe the state of a quantum system. However, it provides a more convenient characterization of a quantum system whose state is not completely known. More precisely, suppose a quantum system can be in one of a number states $|\psi_i\rangle$, with respective probability p_i, where i is an index. We define $\{p_i, |\psi_i\rangle\}$ as an ensemble of pure states. Equation (2.3) defines the density matrix for the system.

$$\rho \equiv \sum_i p_i |\psi_i\rangle\langle\psi_i| \tag{2.3}$$

The density matrix represents a linear operator, also known as the density operator, and both terms are used interchangeably. The density operators are characterized as positive, and if we take the trace of the operator, we end up with the sum of the probabilities of each possible state, which sums to one, $\mathrm{tr}\,(\rho) = 1$. Therefore, the density operator for a quantum system is defined as Positive Semi-Definite (PSD), Hermitian operator of trace one.

This depiction of a quantum state is useful to characterize the amount of known information about the system's state. A quantum system whose state is known exactly is said to be a pure state. More precisely, the density matrix is simply $\rho = |\psi\rangle\langle\psi|$, where $|\psi\rangle$ is the state of the system. Otherwise, ρ is an ensemble of pure states and is said to be in a mixed state. The criterion to identify if ρ is a pure or mixed state, is that a pure state satisfies $\mathrm{tr}(\rho^2) = 1$, while a mixed state satisfies $\mathrm{tr}(\rho^2) < 1$. However, the density matrix depiction highlights when describing the act of a measurement on a quantum system. Quantum measurements are described by a collection $\{\Pi_k\}$ of projective measurement operators. These are operators acting on the state space of the quantum system. The index k refers to the outcome of the projective measurement. If the initial state was $|\psi_i\rangle$, then the probability of getting the result k is given by the Born rule, which for pure states is given by Eq. (2.4).

$$p\,(k|i) = \langle\psi_i|\Pi_k|\psi_i\rangle = \mathrm{tr}\,(\Pi_k|\psi_i\rangle\langle\psi_i|)\,, \tag{2.4}$$

where tr is the trace operator. The operator Π_k is a Positive Operator-Valued Measure (POVM) such that satisfies the completeness equation, $\sum_k \Pi_k = I$. The probability of measuring the result k independent of the initial state of the system is obtained by applying the Bayes' rule on (2.4). So this

probability is given by (2.5).

$$\begin{aligned} p(k) &= \sum_i p(k|i)\, p_i \\ &= \sum_i p_i \operatorname{tr}\left(\Pi_k |\psi_i\rangle\langle\psi_i|\right) \\ &= \operatorname{tr}\left(\Pi_k \rho\right) \end{aligned} \tag{2.5}$$

This is the definition of the POVM version of the Born rule for mixed states. It states that the probability density of observing the system at a given state, when measured, is proportional to the trace of the measured system's density matrix. The Born rule, together with the unitary of the time evolution operator, $e^{-i\hat{H}t}$, implies the unitary of the theory, which is required for consistency.

2.3 Composite Systems

Suppose we have a composite quantum system of two or more distinct physical systems. The state space of this kind of system is the tensor product of the state spaces of the component physical systems. If we have systems numbered 1 through n, and the system i is prepared in the state ρ_i, then the joint state of the total system, ρ, is written as (2.6).

$$\rho = \rho_1 \otimes \rho_2 \otimes ... \otimes \rho_n \tag{2.6}$$

The result of composite systems comes naturally from the principle of superposition of quantum mechanics, which states that for any two states of a quantum system, a superposition of those states should also be an allowed state of the system. For composite systems, if ρ^A is a state of the system A, and ρ^B a state of the system B, then there should be some corresponding state, which we might define $\rho^{AB} = \rho^A \otimes \rho^B$, of the joint system AB. The dimensions of the composite system's state space scale up with the subsystems' state space. If the state space of the subsystem A as a dimension of n, $\mathcal{H}^n$ (Hilbert space of dimension n), and the state space of the subsystem B as dimension of m, $\mathcal{H}^m$, then the total system's state space as a dimension of $n \times m$, $\mathcal{H}^{n\times m}$.

The reduced density matrix is a fundamental tool to describe the subsystems of a composite quantum system. Suppose that we have a composite system of A and B, whose state is described by a density matrix ρ^{AB}. The reduced density matrix for system A is defined by (2.7).

$$\rho^A \equiv \operatorname{tr}_B\left(\rho^{AB}\right) \tag{2.7}$$

Where tr_B is a map of operators known as partial trace over system B. However, sometimes is

not obvious that the reduced density matrix for system A is a description of the state of system A. For example, suppose the composite system in the Bell state (2.2), which is defined by the density matrix ρ'. Tracing out the second qubit, we find that the reduced density matrix of the first qubit is $\rho^1 = \mathrm{tr}_2(\rho') = I/2$. Notice that this state is a mixed state, since $\mathrm{tr}((I/2)^2) = 1/2 < 1$. The state of the composite system of two qubits is a pure state, that is, it is known exactly. However, the first qubit is in a mixed state, of which we do not have full knowledge. Thus, the joint system's state is not separable into a product of its component systems, $\rho^{AB} \neq \rho^A \otimes \rho^B$. Composite systems that have this property are said to be in an entangled state.

2.4 Bell's Inequality

Quantum systems whose state is entanglement have correlation properties that do not match classical physics interpretation. The correlation of entangled states comes from the measurement of one qubit will permanently lock the result of the other qubit, even if the qubits are separated in a causally disconnected manner. These entangled states are also known as EPR pairs, named after a famous paper [2]. However, this paper aimed to dismiss the quantum mechanical interpretation stating that the correlation is due to an intrinsic hidden property of each qubit independent of the measurement. So, even if each qubit can give the value $|0\rangle$ or $|1\rangle$, the measurement's result is predetermined by the hidden property. The interpretation is coherent with classical physics, but it needs a way to be experimentally validated. The result known as Bell's Inequality is the key to experimentally evaluating what type of correlation exists.

Suppose the thought experiment from [5]. A machine prepares two qubits and can repeat the procedure it uses. After preparing, it sends one to Alice and the other to Bob. Alice receives her qubit and measures it. She has two different measurement apparatuses at her disposal, A_Q and A_R, so she can choose which measurement to perform. Both apparatuses can each give one of two outcomes, $+1$ or -1. We denote that Alice's qubit has a value Q if measured by apparatus A_Q and has the value R if measured by apparatus A_R. Similarly, Bob also is capable of measuring using two different apparatus, B_S and B_T, which reveal the result S and T, respectively. Alice and bob do not know which respective apparatus will perform the measurement in advance. The measurement of both qubits is arranged so that Alice and Bob perform it simultaneously (or, more precisely, in a causally disconnected manner). Doing a simple algebra with the quantities of the measurements, we notice the relation (2.8).

$$QS + RS + RT - QT = (Q + R)\,S + (R - Q)\,T \tag{2.8}$$

Since $R, Q = \pm 1$ it follows that either $(Q+R)S = 0$ or $(R-S)T = 0$. In either case, from relation (2.8) results that $QS + RS + RT - QT = \pm 2$. Next, suppose that before the measurements are perform, the

system is in a state where $Q = q$, $R = r$, $S = s$, and $T = t$, with probability $p(q, r, s, t)$. These probabilities may depend on how the machine prepared the qubits and experimental noise. With probability $p(q, r, s, t)$ we can determine a mean value of the quantity $QS + RS + RT - QT$ obtaining the CHSH inequality (2.9).

$$\langle QS\rangle + \langle RS\rangle + \langle RT\rangle - \langle QT\rangle \leq 2 \tag{2.9}$$

Where $\langle\cdot\rangle$ denotes the mean value of a quantity. The CHSH inequality [37] is part of a set of inequalities known as Bell inequalities. After repeating the experiment many times, Alice and Bob can calculate the mean value of each quantity on the left-hand side of (2.9). Thus, CHSH inequality can check if it is obeyed in a real experiment.

Suppose that Alice and Bob perform the following quantum mechanical experiment. The machine prepares the quantum system of two qubits in the state (2.2) and sends the first qubit to Alice and the second to Bob. They measure the arriving qubits using the observables (2.10, 2.11).

$$Q = Z_1 \qquad\qquad S = \frac{-Z_2 - X_2}{\sqrt{2}} \tag{2.10}$$

$$R = X_1 \qquad\qquad T = \frac{Z_2 - X_2}{\sqrt{2}} \tag{2.11}$$

After some calculations, the average values for these observables can be written as $\langle QS\rangle = 1/\sqrt{2}$, $\langle RS\rangle = 1/\sqrt{2}$, $\langle RT\rangle = 1/\sqrt{2}$, and $\langle QT\rangle = -1/\sqrt{2}$. From these values, we arrive at the result (2.12).

$$\langle QS\rangle + \langle RS\rangle + \langle RT\rangle - \langle QT\rangle = 2\sqrt{2} \tag{2.12}$$

The CHSH inequality (2.9) states that the quantity $\langle QS\rangle + \langle RS\rangle + \langle RT\rangle - \langle QT\rangle$ should never be greater than 2. However, quantum mechanics predicts that this sum yields $2\sqrt{2}$. Now one can pose the question: What does the violation of Bell inequality means? There are two main assumptions made to reach Bell inequality: The assumption that the apparatus A_Q, A_R, B_S, and B_T yield definite values Q, R, S, T which are independent of measurement (assumption of realism). The assumption that Alice performs her measurement does not influence Bob's result (assumption of locality). Nevertheless, Bell inequality shows that at least one of these assumptions is incorrect for quantum systems. This result presents an obvious way to distinguish quantum mechanical correlations from classical physics in an experimental way.

3

Entanglement Generation Using Nonlinear Optics

Contents

Nonlinear optics are the phenomena that modify the properties of light when it passes through a material system. Usually, only laser light is intense enough to modify the medium's optical properties. The nonlinearity comes from the material's response depending in a nonlinear manner on the strength of the optical field. More precisely, the polarization density $\vec{P}$ of the medium responds nonlinearly to the presence of an electric field (3.1). The polarization density is defined as the atomic dipole moment per unit volume of the material.

$$P_a = \epsilon_0 \left(\chi^{(1)}_{ab} E_b + \chi^{(2)}_{abc} E_b E_c + \chi^{(2)}_{abcd} E_b E_c E_d + ... \right) \tag{3.1}$$

Where the Einstein summation convention is used to simplify notation. The index a represent the different spatial components of the polarization density tensor P_k. The E_k is the electric field tensor, ϵ_0 is the vacuum permittivity, and the coefficients $\chi^{(n)}$ are the n-th-order susceptibilities tensors of the medium. The second-order and third-order susceptibilities are the most well-known and give origin to key phenomena, such as Spontaneous Parametric Down Conversion (SPDC) ($\chi^{(2)}$) and Spontaneous Four Wave Mixing (SFWM) ($\chi^{(3)}$), that can generate quantum correlated photon pairs. The pairs have different degrees of freedom that can be correlated, such as spatial, frequency and polarization [38]. These photon properties are very suitable to codify quantum information. In this project we aim to generate photon pairs that are entangled in polarization.

3.1 Spontaneous Parametric Down Conversion

The photon pairs are created by an optical process called SPDC, in which a photon spontaneously splits into two other photons of lower energies. The SPDC is a second-order $\chi^{(2)}$ nonlinear process where a photon pumps the medium to generate the photon pairs historically designated as signal and idler. The Feynman diagram in Figure 3.1 schematizes this photon interaction. This kind of optical process naturally happens inside non-centrosymmetric crystals.

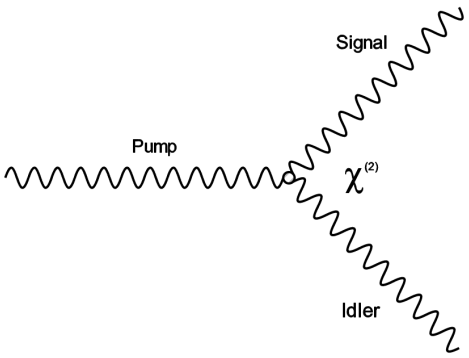

Figure 3.1: Feynman Diagram of the SPDC process.

Assuming the material is non-magnetic and the frequency spectrum of the light is not in resonance with the material's electrons, the process is approximately lossless. Therefore, the rate of change of energy of the electromagnetic field U_{EM} can be expressed using Maxwell's equations for arbitrary dielectrics (3.2). $\boldsymbol{H}$ and $\boldsymbol{B}$ represent the magnetic field and the magnetic flux density field, respectively. Also $\boldsymbol{D}$ and $\boldsymbol{E^{(1)}}$ represent the electric displacement field and the first order electric field, respectively.

$$\frac{dU_{EM}}{dt} = \frac{1}{2}\int d^3r \frac{d}{dr}\left(\boldsymbol{H}\cdot\boldsymbol{B} + \boldsymbol{D}\cdot\boldsymbol{E^{(1)}}\right) + \frac{1}{3}\epsilon_0 \int d^3r \frac{d}{dr}\left(\chi^{(2)}_{psi} E_p E_s E_i\right) + ... \tag{3.2}$$

The indices p (pump), s (signal) and i (idler) represent the different photons present in the interaction. The Hamiltonian of the electromagnetic field is expressed as the sum of a linear optical term (first order) and a nonlinear optical term, $H_{EM} = H_L + H_{NL}$. To understand the interaction is necessary to study it using a quantum optical approach. Quantum optics interpret light as individual photons, quantified energy and momentum of its electromagnetic field, instead of only the wave-like properties. For a more complete understanding of the quantization of the electromagnetic field [39]. The electric field of the pump can be written as (3.3), where the pump mode is aligned with the x axis and treated as a classical monochromatic field of amplitude E_p^0.

$$\boldsymbol{E}_p(\boldsymbol{r},t) = \frac{1}{2}\left[\boldsymbol{E}_p^{(+)}(\boldsymbol{r},t) + \boldsymbol{E}_p^{(-)}(\boldsymbol{r},t)\right] = \frac{1}{2}\left[E_p^0 \boldsymbol{e}_p g_p(\boldsymbol{r})\, e^{-i\omega_p t} + \left(\boldsymbol{E}_p^{(+)}(\boldsymbol{r},t)\right)^{\dagger}\right] \tag{3.3}$$

Here, $\boldsymbol{e}_p$ is the polarization vector, ω_p is the corresponding angular frequency and $g_p(\boldsymbol{r})$ is the spatial distribution of the electric field. Assuming the pump light propagates through the x axis (and the beam is well collimated), the longitudinal dependence can be factored out. So, the wave vectors of the pump $\boldsymbol{k_p}$, signal $\boldsymbol{k_s}$ and idler $\boldsymbol{k_i}$, can be devided into their longitudinal components (k_p^x, k_s^x, k_i^x) and their projections on the transverse plane $\boldsymbol{q_p}$, $\boldsymbol{q_s}$ and $\boldsymbol{q_i}$ (transverse momenta). This means The spatial profile of the incident beam can be defined as (3.4).

$$g(\boldsymbol{r}) = \int d^2q_p G(\boldsymbol{q_p})\, e^{-i\boldsymbol{q_p}\cdot\boldsymbol{r}} e^{-ik_p^x x} \tag{3.4}$$

Where $G(\boldsymbol{q_p})$ is the transverse field distribution in momentum space, which propagates along the x axis of the crystal with transverse momentum $\boldsymbol{q_p}$. The signal and idler photon are quantized as field operators. The displacement scalar operator $\hat{E}_j^{(\pm)}(\boldsymbol{q},t,x)$ in a medium of refractive index n is written as a sum over the momentum modes in a rectangular cavity with volume V and polarization j. This operator (3.5) is separated into two components, a positive frequency $(+)$ and a negative frequency $(-)$.

$$\hat{E}_j^{(+)}(\boldsymbol{q},t,x)=\sum_{\boldsymbol{k}}E_{j\boldsymbol{k}}\hat{a}_{j\boldsymbol{k}}e^{i(\boldsymbol{q}\cdot\boldsymbol{r}-\omega_{j\boldsymbol{k}}t)}e^{ik^x x}=\left[\hat{E}_j^{(-)}(\boldsymbol{q},t,x)\right]^\dagger \tag{3.5}$$

$$E_{j\boldsymbol{k}}=i\sqrt{\frac{\hbar\omega_{j\boldsymbol{k}}}{2\epsilon_0 n_{j\boldsymbol{k}}^2 V}} \tag{3.6}$$

Where $\hat{a}_{j\boldsymbol{k}}$ and $\hat{a}_{j\boldsymbol{k}}^\dagger$ are the annihilation and creation operators for a photon mode with polarization j and wavevector $\boldsymbol{k}=\boldsymbol{q}+k^x\hat{x}$, respectively. Using the derivation of conjugate canonical variables, the quantum Hamiltonian components describing the linear optical effect and the nonlinear optical effects are defined in equations (3.7) and (3.8), respectively. Notice that the linear Hamiltonian can not be responsible for the creation of photon pairs, as it only depends on the first order creation and annihilation operators.

$$\hat{H}_L=\sum_{\boldsymbol{k}}\hbar\omega_{j\boldsymbol{k}}\left(\hat{a}_{j\boldsymbol{k}}^\dagger\hat{a}_{j\boldsymbol{k}}+\frac{1}{2}\right) \tag{3.7}$$

$$\hat{H}_{NL}=\epsilon_0\frac{1}{3}\int d^3r\chi_{psi}^{(2)}\boldsymbol{E}_p\hat{E}_s\hat{E}_i \tag{3.8}$$

The SPDC process can be divided into three types depending on the polarization of the interacting waves. Type 0 is where the signal and idler have the same polarization as the pump photon. Type I is where the photon pair has the same polarization and is orthogonal to the pump. Finally, type II is where the photon pair have orthogonal polarization in relation to one another. In this work, we will address the type II SPDC. The nonlinear Hamiltonian (3.8) is the sum over eight distinct terms, which the combination of those terms correspond to different nonlinear optical effects. However, only those processes that conserve energy contribute significantly to the probability amplitude of down conversion. For many nonlinear media, $\chi^{(2)}$ is only significant for one particular optical process which can be engineered by design. The susceptibility tensor contracts with the unit vectors of the field operators, so it can be reduced to a scalar effective nonlinear coefficient, $\chi^{(2)}\boldsymbol{e}_p\boldsymbol{e}_s\boldsymbol{e}_i=\chi^{(2)}\hat{z}\hat{z}\hat{y}=\chi_{eff}^{(2)}$. The vertix of the interaction (Figure 3.1) describes that in the SPDC process either pump photons are destroyed in exchange for signal-idler photon pair creation, or vice versa. Therefore, the nonlinear Hamiltonian is well approximated to the Hamiltonian of the SPDC process, which becomes (3.9).

$$\hat{H}_{NL}\sim\hat{H}_{SPDC}=-\frac{\chi_{eff}^{(2)}\hbar E_p^0\sqrt{\omega_i\omega_s}}{Vn_sn_i}\sum_{\boldsymbol{k}_s,\boldsymbol{k}_i}\Phi(\Delta\boldsymbol{k})\,e^{-i\Delta\omega t}\hat{a}_{\boldsymbol{k}_s,\omega_s}^\dagger\hat{a}_{\boldsymbol{k}_i,\omega_i}^\dagger+\text{h.c.} \tag{3.9}$$

$$\Phi(\Delta\boldsymbol{k})=L\int d^2q_pG(\boldsymbol{q}_p)\,\delta(\Delta q_x)\,\delta(\Delta q_y)\,\text{sinc}\left(\frac{\Delta k^xL}{2}\right)=LG(\boldsymbol{q}_s+\boldsymbol{q}_i)\,\text{sinc}\left(\frac{\Delta k^xL}{2}\right) \tag{3.10}$$

Where $\Phi(\Delta \boldsymbol{k})$ is the SPDC biphoton mode function. Here, we also introduce the frequency mismatch $\Delta\omega = \omega_p - \omega_s - \omega_i$ and the wavevector mismatch $\Delta \boldsymbol{k} = \boldsymbol{k}_p - \boldsymbol{k}_s - \boldsymbol{k}_i$. In most experimental setups, the nonlinear medium is a simple rectangular crystal centered with side lengths L_x, L_y and L_z. Also, the term h.c. means the hermitian conjugate. In the Schrödinger picture, with a defined Hamiltonian it is possible to determine the time evolution of the initial state $|\Psi_{\text{initial}}\rangle$ over a time T. The final state is then obtain by (3.11) where the initial state is a composite system of a pump photon, with wavevector $\boldsymbol{k}_p$ and angular frequency ω_p, and two vacuum states for the signal and idler photons.

$$|\Phi_{\text{final}}\rangle = e^{-\frac{i}{\hbar}\int_T dt \hat{H}_{SPDC}} \left[|\boldsymbol{k}_p, \omega_p\rangle_p \otimes |\text{vac}\rangle_s \otimes |\text{vac}\rangle_i\right] \tag{3.11}$$

Assuming that the interaction strength is small, the exponential can be expanded and anything beyond the second term is discarded. Discarding the higher order terms represent that is not possible for one pump photon to generate multiple photon pairs. Extending the integration limits to infinity ($T \to \infty$), we get the steady state solution of the final state. Finally, the solution of the final state of the SPDC process where a pump photon generated a photon pair signal-idler, is written as (3.12).

$$|\Psi\rangle_{s,i} \propto L\frac{\chi^{(2)}_{eff}\hbar E_p^0}{V}\omega_s \frac{\sqrt{\frac{\omega_p}{\omega_s}-1}}{n_s n_i} \iint d\boldsymbol{k}_s d\boldsymbol{k}_i \,\text{sinc}\left(\frac{\Delta k^x L}{2}\right) G\left(\boldsymbol{q}_s + \boldsymbol{q}_i\right) |\boldsymbol{k}_s, \omega_s\rangle |\boldsymbol{k}_i, \omega_p - \omega_s\rangle \tag{3.12}$$

The Hermitian conjugate term of the Hamiltonian as disappear, since it is composed of annihilating operators acting on the vacuum. Note that this result shows that the signal and idler photons are only produced in pairs. This interaction type has been well studied and documented [40]. The photons produced may or may not have the same energy. In the case that both photons have the same frequency ($\omega_s = \omega_i = \omega_p/2$), the photons are called degenerate. When the photons have different frequencies, the photons are non-degenerate.

$$\begin{aligned} \Delta\vec{k} &= \vec{k}_p - \vec{k}_s - \vec{k}_i = 0 \\ \Delta\omega &= \omega_p - \omega_s - \omega_i = 0 \end{aligned} \tag{3.13}$$

The correlation of the photon pair, created by the SPDC process, comes from the conservation laws of energy and momentum dictated by the Phase Matching (PM) conditions. To satisfy the PM conditions, the mismatch wavevector Δk and the mismatch energy $\Delta\omega$ must be zero (3.13). In this case, the atomic dipoles that constitute the material are properly phased so that the field emitted by each dipole adds coherently in the forward direction. This way, the generated waves can extract energy most efficiently from the incident wave since the total power radiated by the atomic dipoles scales as the square of atoms that participate [1]. According to the sinc function in 3.12, the generated wave intensity deeply

depends on the mismatch wavevector, which decreases dramatically when the perfect PM, $\Delta k = 0$, is not satisfied. This condition dictates that the waves interfere constructively up to a particular coherent length L_{coh} of the crystal.

For nonlinear mixing processes, the PM conditions are often difficult to achieve because of the normal dispersion of the material since the refractive index depends on the frequency, ω, of the light, as in the example shown in Figure 3.2. However, using the birefringence displayed in some mediums, one can achieve the PM conditions. Birefringent crystals have different refractive indexes depending on the direction of polarization of light. The value of the effective refractive index of the material depends on the direction of polarization of the pump, signal and idler photons with respect to the optical axis of the crystal. So, the PM conditions can be satisfied by tuning the crystal's temperature or the angle between the incident pump wave and the optical axis of a nonlinear birefringent crystal.

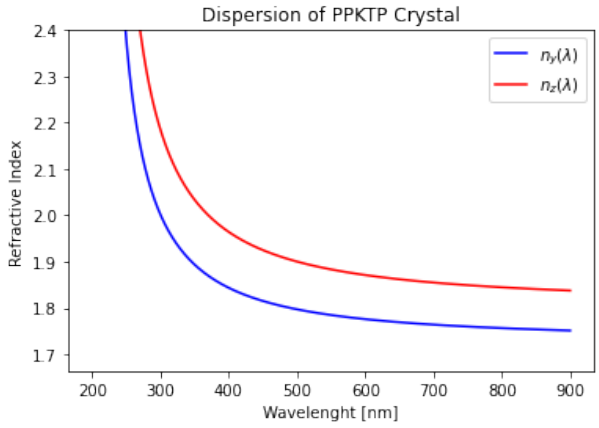

Figure 3.2: Dispersion of the refractive index for a KTP crystal at different directions of light propagation. The blue curve represents the refractive index in the y direction and the red curve represents in the z direction. Details on the dependence of the wavelenght λ are found in Appendix A.1.

However, PM by angle tuning is not always possible. For type 0 and type I SPDC, the birefringence of the crystal does not affect the temporal profile of the photon pair because both signal and idler have the same polarization. In this case, PM is achieved by tuning the crystal's temperature. For type II SPDC, this effect affects the photon pair's direction of propagation and differentiates their temporal profile.

3.2 Quasi Phase Matching

Section 3.1 describes the use of birefringent optical materials to achieve the PM condition of nonlinear optics. However, there are circumstances in which this technique is not suitable. For Example, if the material possesses low birefringence to compensate for the dispersion of the refractive indices. In this case, the PM conditions can be satisfied using a technique called Quasi Phase Matching (QPM). This technique is based on the manipulation of the nonlinear coefficient d_{33} of the $\chi^{(2)}$ tensor. The

Figure 3.3 illustrates the idea of QPM, where Figure 3.3(a) represents the structure of a Periodically Poled (PP) material, and Figure 3.3(b) represents the coupling coefficient as a function of the position of the material. A PP crystal is fabricated in such a manner that one of the crystalline axes (often the c axis of the ferroelectric material) is inverted periodically along the length of the crystal.

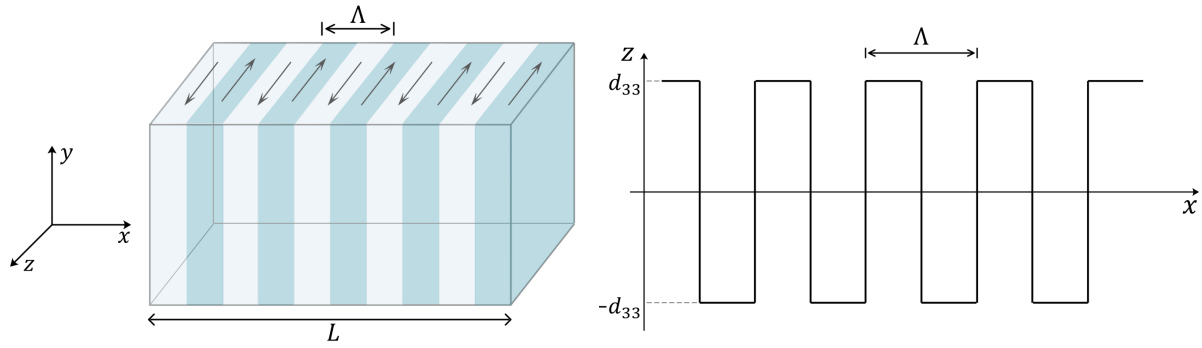

(a) Representation of the grating structure **(b)** Graphic of the nonlinear coupling coefficient $d(x)$

Figure 3.3: Graphic representation of a periodic poled crystal with period of poling Λ and lenght L.

The nonlinear coefficient tensor d_{abc} is related to the second-order nonlinear susceptibility as $d_{abc} = \frac{1}{2}\chi^{(2)}_{abc}$. Normally, the susceptibility depends on the frequency of the electric fields. However, often nonlinear optical interactions involve light waves whose frequencies are much smaller than the lowest resonance frequency of the material system. Under these conditions, the nonlinear susceptibility is essentially independent of the frequencies of the applied waves. Furthermore, under the conditions of low-frequency excitation, the system responds without loss to the applied field. This condition is known as Kleinman symmetry. Assuming that the Kleinman symmetry is valid, the nonlinear tensor d_{abc} becomes symmetric in the last two indices and can be rewritten as a contracted matrix d_{ad} where the coefficient d_{33} is located. A mathematical description of the spatial dependence of the nonlinear coupling coefficient is simply the square-wave function (3.14), as shown in Figure 3.3(b).

$$d(x) = d_{33}\,\mathrm{sign}\left[\cos\left(\frac{2\pi x}{\Lambda}\right)\right] \tag{3.14}$$

The grating structure of the material inverts the sign of the nonlinear coupling coefficient d, with period $\Lambda = 2L_{coh}$, which gives an extra wave-vector to the PM conditions, $|\vec{k}_g| = \frac{2\pi}{\Lambda}$. Thus, the mismatch wavevector Δk writes as quasi-phase-mismatch (3.15).

$$\Delta\vec{k}_{QPM} = \vec{k}_p - \vec{k}_s - \vec{k}_i - \vec{k}_g \tag{3.15}$$

Every pole alternation accumulates a π phase creating the $\vec{k}_g$, and this vector depends on the L_{coh} to compensate for the mismatch. Then L_{coh} can be defined as $L_{coh} = \frac{\pi}{|\Delta\vec{k}|}$ [1]. The nature of these

effects is illustrated in Figure 3.4. The curve (a) of the figure shows that with perfect PM, $\Delta k = 0$, the field strength of the generated wave grows linearly with propagation through the medium. The curve (c) shows that with the presence of a mismatch vector, $\Delta k \neq 0$, the generated field amplitude oscillates with propagation distance, which demonstrates that the field amplitude at any point in the material will never be greater than the amplitude at L_{coh}. Adding an extra wavevector $\vec{k}_g$ corrects the mismatch vector Δk each time the field amplitude is about to decrease, which allows it to continue to grow monotonically. Thus, a longer PP crystal increases the amplitude of the generated field with the length, as shown in curve (b). This phenomenon was predicted by Armstrong et al. [41] and was later demonstrated by Kwiat et al. [42].

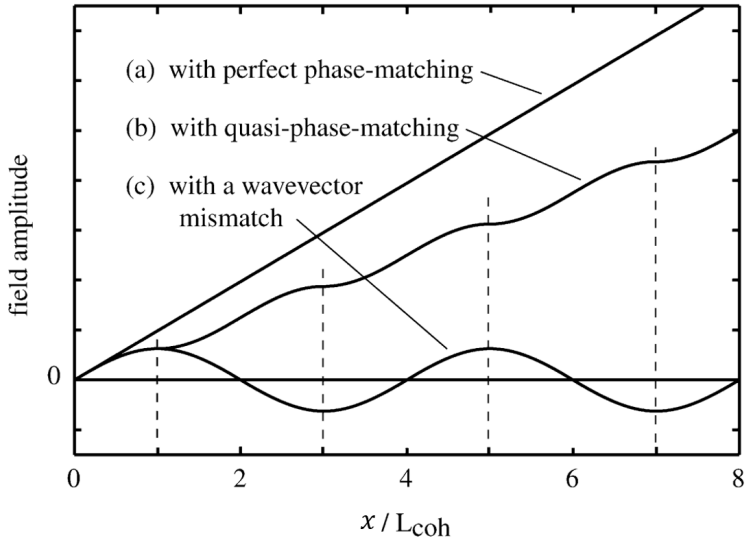

Figure 3.4: Electric field amplitude of the photon pairs generated by SPDC as a function of the length of the crystal. Curve (a) assumes perfect phase-matching. Curve (c) assumes quasi-phase-matching where the orientation of the crystalline axis switches with a period twice the coherent length L_{coh}. Curve (c) assumes phase mismatch. Figure from [1].

The QPM conditions restrict the behavior of the nonlinear process and gives a dependence between all parts of the interaction. In appendix A.2 we adress more precisely the relation between wavelengths and the propagation orientation of the photon pairs with the temperature of the medium.

3.3 Entangled State of Two Photonic Qubits

The photon pairs polarization can be interpreted as composite system of two qubits. Where the polarization in the horizontal direction ($|H\rangle$) is labeled $|0\rangle$ and the polarization in the vertical direction ($|V\rangle$) is labeled $|1\rangle$. The photon's polarization has all the properties of a qubit, since can be in any superposition of the polarization's linear basis $|H\rangle, |V\rangle$. Thus, a pair of photons can create a system of two qubits in a composite state which the measurement outcomes cam be $|HH\rangle$, $|HV\rangle$, $|VH\rangle$ or $|VV\rangle$.

Photon pairs behave as a composite system, so is possible to create entangled states with the polarization of the photon pairs. Figure 3.5 shows one way to produce an entangled state from a photon pair, each one with distinct polarization.

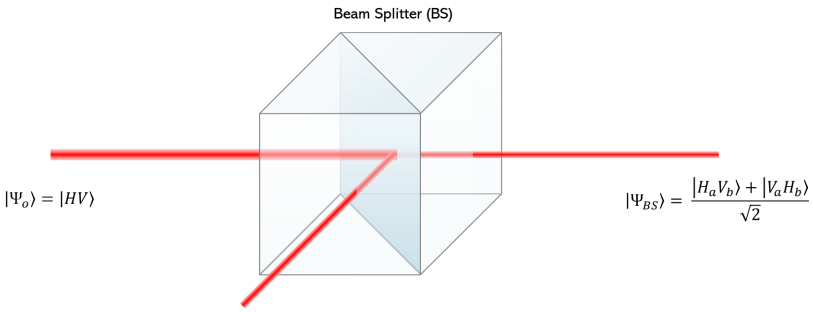

Figure 3.5: Schematic of photon pair interaction with BS. The state before the interaction is $|\Psi_0\rangle$ and the final state is $|\Psi_{BS}\rangle$. Note that final state only considers the photons end up in separate paths.

Suppose that we have two photons produced by a type II SPDC. The process is pumped by a horizontal polarized photon $|H\rangle$, which the system state after the interaction becomes $|HV\rangle$, where the first photon is the signal and the second is the idler. Assume that both photons are completely indistinguishable except in polarization. Sending this state through a $50:50$ Beam Splitter (BS) each photon can be reflected or transmitted with $1/2$ of probability for each case. So, after the photon pair interacts with BS and each photon go in a different path, the systems state becomes 3.16.

$$|\Psi\rangle = \frac{|HV\rangle + |VH\rangle}{\sqrt{2}} \tag{3.16}$$

Where the first qubit is the polarization of the photon that was transmitted and the second qubit is the one reflected by the BS. Notice that both photons are correlated so that we know that they are of opposite polarization, however, we can not know which path signal and idler goes. This is a polarization bell state equivalent to 2.2. Though, this technique does not always work, in fact only works 50 % of the times, because there are also the possibility that both photons choose the same path (bunching). But by detecting the presence of a photon in each path, we can identify the bunching cases and neglect it.

4

Photon Pair Source Setup

Contents

The main objective of my Master project is to plan and build a photon pair source in laboratory. The source generates entanglement photon pairs via SPDC process. The photons emitted by the laser, and used to pump the non linear crystal, will have twice the frequency of the generated pairs, hence half the wavelength. This is a probabilistic phenomenon, which means that there is a certain probability to generate a (or even multiple) pair of photons per pump pulse. This process ends with a light beam containing pump photons that were not down converted and photon pairs generated inside the crystal. In order to only have at the exit correlated photon pairs we include a bunch of filters to remove the presence of pump photons in the beam. Figure 4.1 shows a schematic of the experimental setup that we implemented in this project.

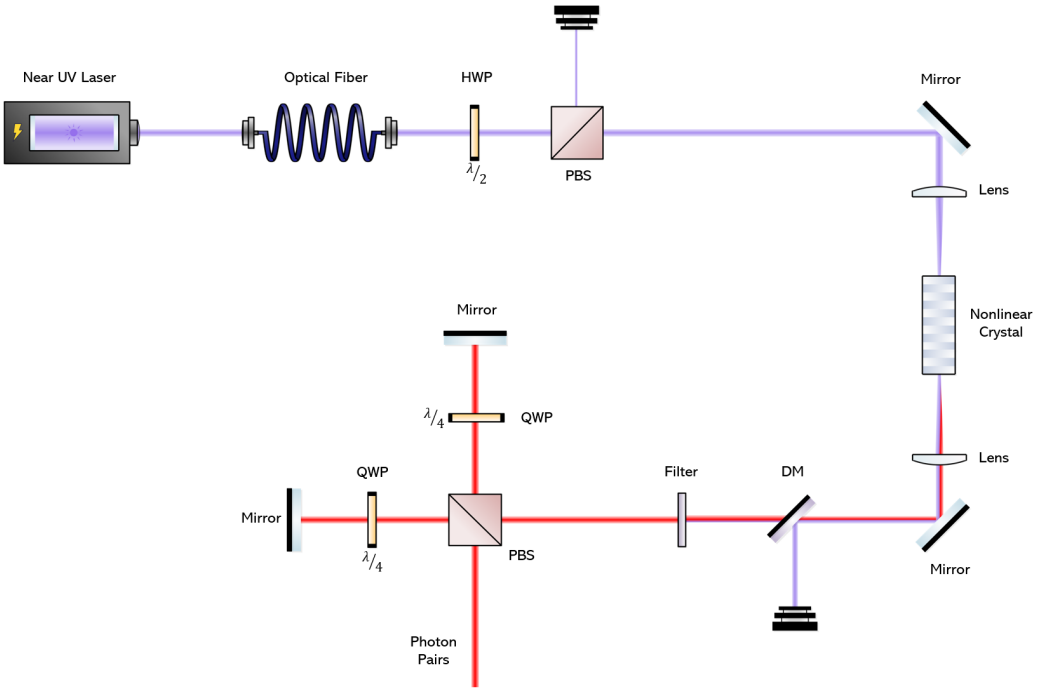

Figure 4.1: Schematic of the experimental setup.

The setup starts with a laser that pumps all the rest of the optical circuit. Before pump reach the nonlinear crystal, the light beam requires that its spatial profile to be a clean Gaussian with a single direction of polarization to generate efficiently photon pairs. The pump is down converted into photon pairs inside a Periodically Poled Potassium Titanyl Phosphate (PPKTP) crystal that is placed inside a oven to control its temperature. After the crystal we block only the pump light with low frequency pass filters and mirrors, to only have correlated pairs at the exit of the setup. For the photon pairs to be optimized for entanglement they need to be indistinguishable except for polarization. However, because of the birefringence of the crystal, the signal and idler will experience different refractive indexes, hence the medium creates a time difference between them. To overcome this condition we use a Hong-Ou-Mandel (HOM) interferometer to separate both photons, correct the time delay and recombine them in

the same beam. This way, at the end of the setup we have a beam of indistinguishable photon pairs.

4.1 Pump Light Source

The first section of the experimental setup is projected to generate and prepare a mono-mode single frequency pump light beam. Figure 4.2 shows a schematic of the pump section. A laser produces a near Ultra Violet (UV) light beam that then is coupled inside a optical fiber to remove the spatial modes affecting the Gaussian profile of the beam. To make the down-conversion process more efficient, we clean out the non-horizontal modes of polarization before sending the beam to the crystal. For that we use a Half Wave Plate (HWP) and a Polarization Beam Splitter (PBS) that selects and maximizes the output of horizontal polarization photons.

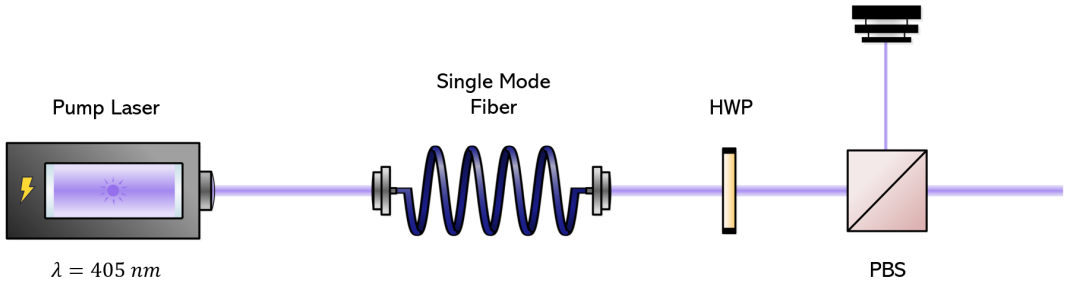

Figure 4.2: Schematic of the pump section.

The laser at the beginning of the setup is a compact laser diode from Ondax, that emits a light beam with 405 nm of wavelength (near UV light). The laser's temperature is tunable, so that changes the spatial profile of the beam. Also the power of the beam is tunable by changing the current of the laser. At the initial stage of the experimental setup, the laser is at 25℃, and emits a near UV beam with 57.6 mW of power that is focus inside a single mode optical fiber. These fibers are design to propagate only the fundamental transverse mode of light and attenuate higher order modes. For a Gaussian beam laser, the surviving mode inside the fiber is TEM_{00} [43]. The fiber used in the setup as approximately 24% of coupling, so the light beam's intensity decreases inside the fiber and exits with 13.8 mW. After the fiber, the pump light beam has TEM_{00} spatial mode and is sent through a HWP followed by a PBS to filter out the non horizontal polarization modes.

The PBS separates deterministically the vertical polarization photons ($|V\rangle$) from the horizontal ($|H\rangle$) by letting the beam pass through a coating that reflect the vertical to one direction and let transmit the horizontal to other direction. Thus, in the direction of the propagation of the setup we only have horizontal polarized light. The HWP rotates the polarization over the linear axis, this happens due to different

refraction indexes of the medium in each Cartesian direction. Controlling the HWP we can maximize the number horizontal polarized photons that passes through the PBS. The apparatus composed by HWP and PBS is placed following the fiber so that the horizontal polarization is not lost. The a pump beam after the PBS as a power of 10.7 mW, which means that 32% of the laser couldn't be converted to horizontal polarization.

4.2 Photon Pair Generation

The pump laser, after been prepared as stated in previous section, is focused inside the nonlinear crystal with a plano-convex lens with focal distance of 7.5 mm. The beam is focused to increase the intensity inside the crystal to make the SPDC process more efficient. The crystal used in the setup is a PPKTP ($KTiOPO_4$) from Raicol Crystals. It as dimensions of $1 \times 2 \times 30$ mm, is birefringent and as PP period of $\Lambda = 10$ μm. The crystal's coherence length, L_{coh}, is determined by the value of Λ and is 5 mm. For a PP crystal, the nonlinear processes becomes more efficient when the pump beam propagates in the medium for a distance bigger than L_{coh}. The amplitude of the generated field of photon pairs is approximately five times bigger than the maximum field generated by a non PP crystal. The SPDC interaction that happens inside the crystal is of type II, which means that the electric fields $\vec{E}_p$ and $\vec{E}_i$ are polarized in the ordinary axis ($|H\rangle$), and the electric field $\vec{E}_s$ is polarized in the extraordinary axis ($|V\rangle$). For this type of process inside a PPKTP crystal, the conversion efficiency is estimated to be 9.5×10^{-9}% [44]. The crystal's refractive index not only differs with the direction of propagation (birefringence) but also varies with its temperature (see Appendix A.1). So the crystal is placed inside an oven that controls its temperature and maintain constant through all the process. At the exit of the crystal we expect a beam of light composed of non converted pump photons (405 nm) and down converted photon pairs (810 nm). The photon pairs generated inside the crystal are in the spectrum of Infra Red (IR) light. The beam outside the crystal have 7.3 mW, which means that there are a decrease of 3.4 mW of pump intensity. This means that approximately 3×10^{-8}% of the missing pump was converted to photon pairs, and the rest was lost due to internal reflections inside the crystal's oven. The majority of power loss happens inside the crystal, besides the setup being optimized, the SPDC process is still the most inefficient part of the experiment.

After passing through the crystal, the light beam is collimated using a second plano-convex lens with focal distance of 125 mm. The light beam at this stage is composed already of correlated photon pairs. However, to use it we have to remove the residual pump photons from the main beam. For that we use a frequency band-pass filter that absorbs and reflects light with wavelength outside the 800 ± 40 nm. To reinforce this effect we add a Dichroic Mirror (DM) to reflect only the high frequency photons and transmit the down converted photons. Finally, at the end of this setup's section we have a collimated

light beam mostly composed of IR photon pairs.

4.3 Hong-Ou-Mandel Interferometer

The photon pairs, when produced inside the crystal, have to propagate through a birefringent medium. Because of type II SPDC, the signal and idler photons have different polarization modes, horizontal and vertical, respectively. Thus, the photon pairs will exit the crystal at different times. This phenomenon creates a time delay between both photons, and this makes the photons distinguishable in time. Now, at the exit of the crystal the photon pairs are in state $|H, t_1\rangle_s \otimes |V, t_2\rangle_i$ where the delay is $\Delta = |t_1 - t_2|$. To make them indistinguishable in time the delay must be zero. So, we must compensate the temporal profile of one of them in such way that $t_1 = t_2$. For that we use a HOM interferometer represented in Figure 4.3. The purpose of HOM is to separate both photons into two different path, one longer than the other, and at the end recombine them again in the same beam. The difference in length of the paths creates a slight temporal delay that can compensate the one created by the crystal. After the interferometer recombines both photons, the system's state becomes $|VH\rangle$.

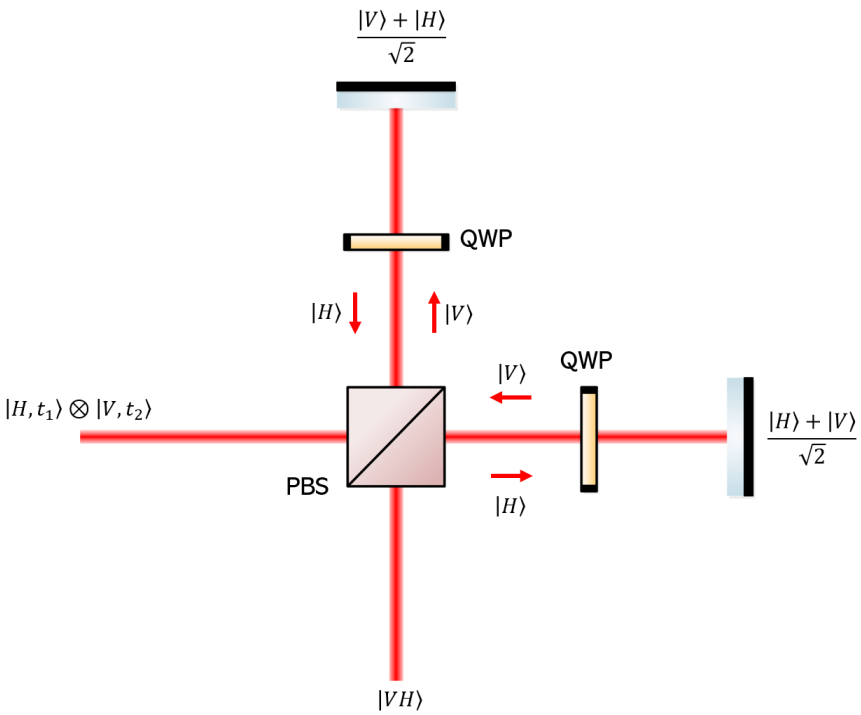

Figure 4.3: Shcematic of the HOM interferometer.

The HOM interferometer separates deterministically the incoming state of the photon pair using a PBS. The signal photon which has horizontal polarization is transmitted through the PBS to one arm of the interferometer, and the idler photon (vertical polarization) is reflected by the PBS to the other arm.

Both photons must propagate through the arm two times because of the mirrors at the end of the path, and recombine in the PBS. One of the arms has a slightly different length, so the photon in that path will be delayed by δ/c seconds, where δ is the difference of the length of both arms. In midway of both paths there is a Quarter Wave Plate (QWP), this optical component rotates the polarization by $45°$. Thus, a round trip in each arm will rotate the photon polarization by $90°$, transforming horizontal polarization into vertical and vice versa. When photons reach again the PBS, they have inverted polarization, so they will recombine in a different path that they enter the interferometer, but now with indistinguishable temporal profile. The final output of the source is a IR light beam with count rate of 2.6×10^6 single photons per second, which results on a production rate per mW of pump of around 45.14 $\frac{\text{kHz}}{\text{mW}}$.

5

Characterization of the Photon Pair Source

Contents

In this chapter, we experimentally characterize key properties of the source and optimize the quality of the entanglement. First, we characterize the spatial profile of the beam throughout the setup to ensure the beam is approximately Gaussian and collimated. To characterize the photon pairs, we analyse photon statistics of the output of the crystal. For such measurements, we build an electronic coincidence detector to measure the distribution of the photon pairs, and we also use a state of the art time tagger. Using these tools, we measure the HOM dip to determine the temporal deviation of the pairs, and compensate it using a movable mirror. Finally, we experiment with Bell state measurements to certify entanglement via the violation of a Bell inequality.

5.1 Spatial Profile Characterization

In this section, we characterize the beam's spatial properties at different points of the setup shown in (Figure 4.1). We aim to study the spatial shape of the beam through out the setup. The spatial profile desired for the light beam is the fundamental Gaussian transverse mode TEM_{00}. The pump beam exiting the laser has a superposition of different spatial modes that together make a complex, non-Gaussian, profile. The purpose of the single mode optical fiber is to clean these modes and modulate it closer to a Gaussian beam, in other words it acts as a spatial filter. Figure 5.1 shows the beam profile before (Figure 5.1(a)) and after (Figure Figure 5.1(b)) the beam passes through the fiber. Both figures where taken using a scanning-slit optical beam profiler from Thorlabs. The profile before entering the fiber has an elliptical Gaussian mode (with eccentricity of 63.71 %) due to the additional spatial modes. After the fiber the spatial profile is closer to a circular Gaussian mode (with eccentricity of 15.77 %).

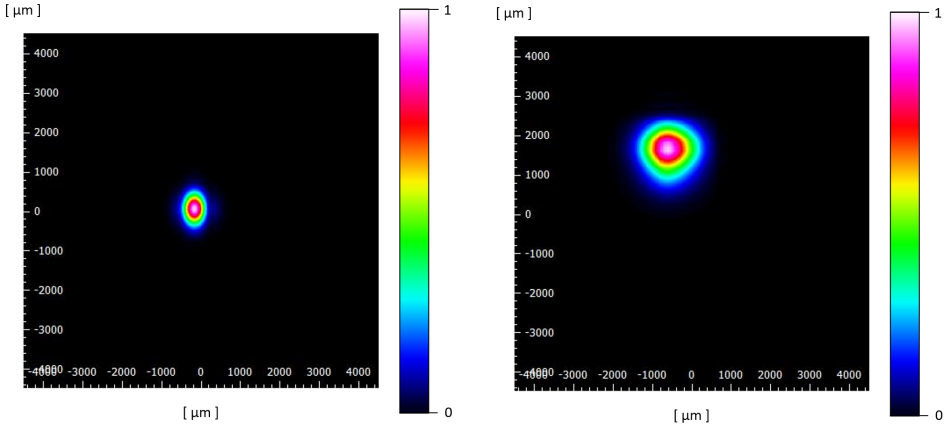

(a) Beam profile before single mode fiber. **(b)** Beam profile after single mode fiber.

Figure 5.1: Comparison of the pump beam profile before and after passing through the single mode fiber. Images taken with beam profiler.

The pump is focused using a plano-convex lens to make the conversion process more efficient. The minimum beam waist inside PPKTP crystal is 0.3593 mm. At the exit of the crystal, the beam is composed of pump light and converted light. Figure 5.2 shows the spatial profile of the residual pump after the nonlinear process (Figure 5.2(a)) and the photon pairs (Figure 5.2(b)). The images were taken using a Charge-Coupled Device (CCD) from Thorlabs. Since the conversion efficiency is very low, the pump's intensity is much higher comparing to the intensity of the pairs. So, to observe both profiles, we took a direct picture of the crystal's output beam, and another picture with a frequency band-pass filter to remove the pump photons. The pairs profile is close to a Gaussian profile, where residual pump beam lost the circular profile after interacting with the crystal. Analysing the centroid of both profiles, we measured the relative emission angle between the pump and the pairs of $0.2076\,°$, which is very close to collinear.

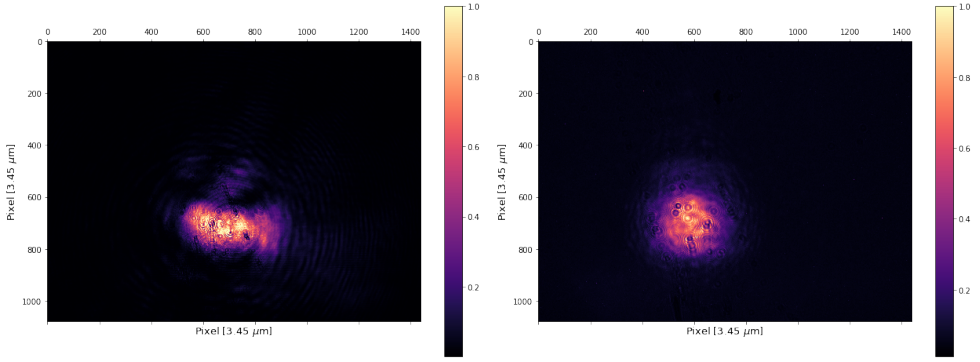

(a) Beam profile without a filter.

(b) Beam profile with a filter.

Figure 5.2: Image of the photon pairs at the exit of the crystal with and without a 810 nm filter. Image taken with CCD camera.

The light beam at the output of the crystal is collimated using a plano-concave lens. The goal is to minimize the output beam's divergence. Using the CCD camera, we also took snapshots of the beam's profile at different distances, and with the estimated beam waist variation, we determine the divergence of the photon pairs beam. The beam radius diverges with an angle of $0.0211\,°$. As an illustrative example, the beam's diameter increases to around 1 cm after propagating 26 m.

5.2 Time Correlated Single Photon Counting

The Time Correlated Single Photon Counting (TCSPC) is a well established technique to make measurements on the optical time domain [45]. The principle of TCSPC is the detection of single photons and the measurement of their time arrival. The objective is to use this method to record the arrival of a photon pair and distinguish those detections from background photons events (dark counts). This tech-

nique is a statistical method that requires a high repetitive light source to accumulate a sufficient number of photon events for data precision. To register the time at a photon arrives a detector, the TCSPC needs a periodic excitation signal of reference, with very low probability of registering more than one excitation per cycle. One can verify the sparseness of the collected photons and reconstruct the temporal profile of the pairs from the multitude of single photon events collected over many cycles. The time difference between the photon arrival and the reference signal is measured by electronics that act like a stopwatch. The readings of the electronics are sorted into a histogram. The width of the time bins of the histogram correspond to the time resolution of the stopwatch. For optical processes, very small timing resolutions are required. Typically photon events are detected in the order of picoseconds and need a very fast stopwatch to achieve a good quality measurement. For detection of single photon events, usually avalanche photodiodes are used, incorporated in Single Photon Counting Modules (SPCMs). When detecting a single photon, this module emits an electrical pulse that is processed by the TCSPC. To characterize the temporal profile of the photon pairs emitted by the experimental setup, we use two SPCMs, one from Excelitas and another from Laser Components.

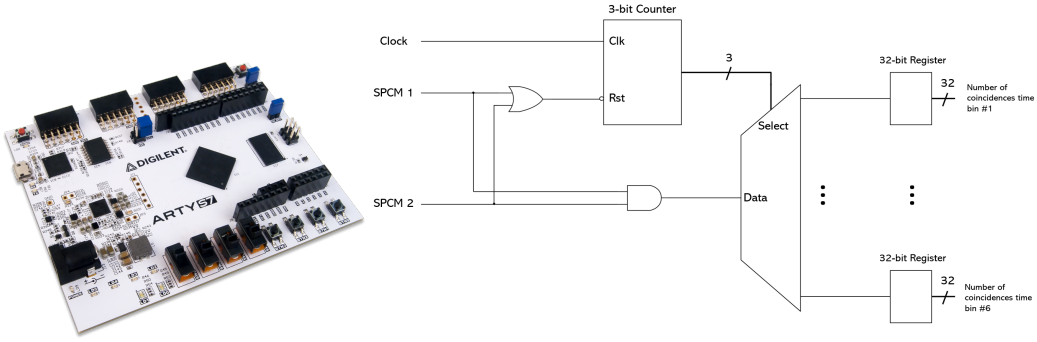

(a) Xilinx's Artix-7 25 FPGA Board.

(b) Schematics of the circuit implemented on the FPGA.

Figure 5.3: TCSPC's digital circuit implemented on the FPGA.

The electronics of the TCSPC were mounted in a Field Programmable Gate Array (FPGA) board by Xilinx (Figure 5.3(a)). The SPCM are connected to the FPGA board at pmod ports. The circuit inside the FPGA creates a histogram depending on the time difference of the pulses emitted by the modules. Figure 5.3(b) shows the schematic of the digital circuit inside the FPGA. When the first electrical pulse arrives at the FPGA, it will start a counter of 4-bits. The counter's incrementation rate is controlled by the FPGA's clock, which works as a reference signal. The arrival of the second pulse will activate an AND gate which sends a signal through a demultiplexer. The output of the demultiplexer is controlled by the value of the counter which was started by the first pulse. Hence, the outcome of the demultiplexer depends on the time difference of both electrical pulses. Each exit of the demultiplexer is connected to

a register that will increment the counter each time a signal arrives. The register will save the number of events at the respective time bin. Reading the values of all registers gives us the histogram. The time bin width is determined by the period of the reference signal, which for Xilinx's FPGA is $2,5$ ns (clock's frequency is 400 MHz). The maximum delay between two pulses that can be detected depends on the width of the longest pulse. The detectors pulses have a width of 10 ns (Excelitas) and 15 ns (Laser Components), which means that the maximum delay is 15 ns. The histogram generated by this TCSPC have 6 time bins.

To test the precision of the measurements of the FPGA, we connected the pmod inputs to a Wave Function Generator (WFG). To simulate the pulses from the detectors, the WFG emits a two square wave functions with a fixed temporal delay. Figure 5.4 shows the results of the test for two distinct delays, 5 ns and 12 ns, respectively. There is a clear difference in the histogram for each delay, but the histograms don't not show a predominant time bin. For fixed delay, we expected a much bigger number of counted events in the respective time bin, however that was not verified. This is due to two factors: the dark counts of the SPCM that create noise in the measurement circuit, and the temporal delays inside this particular FPGA chip which cannot be controlled.

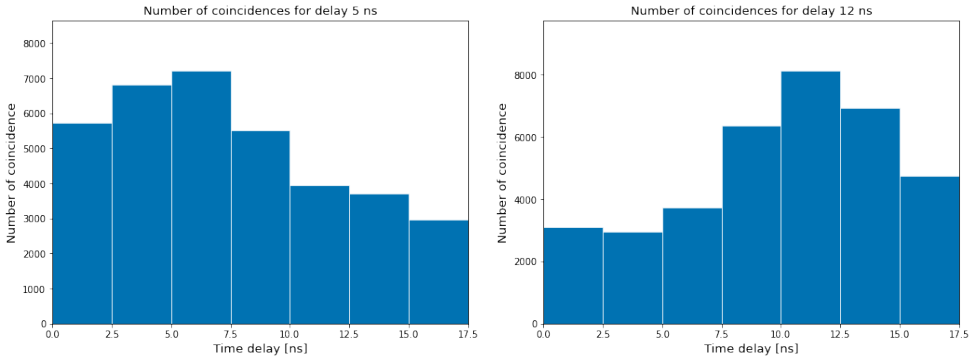

(a) Coincidence Histogram for 5 ns of delay.

(b) Coincidence Histogram for 12 ns of delay.

Figure 5.4: Measurement tests for two signals with two different delays.

The following characterization measures the number of coincidences registered by the SPCM. A coincidence is defined as an event that contributes to the lowest time bin of the TCSPC, and the coincidence window is given by the time resolution. The FPGA has a coincidence window of 2.5 ns which is not very precise for the characterization of the photon pair source, but could still in principle be used for that application. However, near the end of my Master project, the laboratory acquired a professional time tagger (Swabian Instruments) that works as TCSPC. The time tagger has much faster electronics and a time resolution of approximately 40 ps. The histogram generated by the time tagger has a total of 1000 time bins each one with a width of 40 ps. In Figure 5.5 is an example of an histogram from

Section 5.3 with the movable mirror at position 0. Nevertheless, the code I wrote is a good starting point for the laboratory to use FPGAs in the future, which is also important for quantum key distribution. The results reported in the following section were obtained using the new time tagger device.

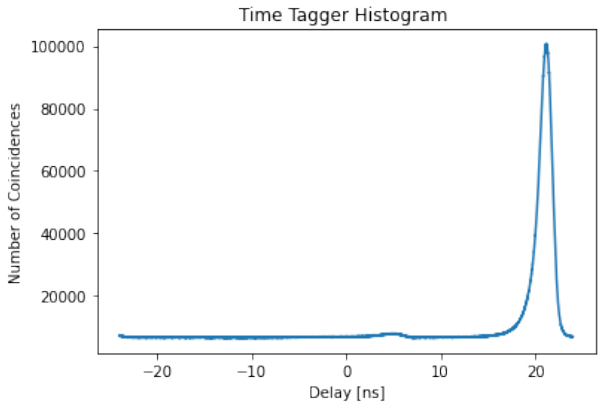

Figure 5.5: Time tagger histogram with asymmetrical delay of 21.18 ns.

In a perfect system the time of coincidence of the detection of both photons is at 0 delay. However, there is a delay imposed not only by the birefringence of the crystal but also by the asymmetry of the paths after the BS. This asymmetry comes from differences in length between the paths after the BS and before the fibers, differences in the lengths of the fibers, and also differences in the length of the cables that connect the SPCM to the time tagger. The experimental setup has asymmetrical delay of 21.18 ns. This is a fixed delay, and can be electronically compensated.

5.3 Temporal Characterization

The photon pairs are emitted from the crystal with a time delay between them, as explained in Section 4.3. Hence, after generating the photon pairs and eliminating the residual pump light, we use a HOM interferometer to compensate the delay. The HOM is used to measure the delay, so we know where to place the mirror. The HOM interferometer is based on a effect with the same name [46]. The effect states that two completely indistinguishable photons interfere with each other when interacting with a BS. The outcome quantum state has the special property that isn't possible to detect the presence of a photon in both arms of the BS. In other words, the two indistinguishable photons bunch (both photons go to the same detector) after interacting with a BS. Hence, the coincidences of both detectors measure the presence of a photon drop to zero. The experiment in Figure 5.6 measures the time delay of the photon pairs using the HOM effect.

The characterization experiment tests the time delay between the photon pairs by moving the mirror in the HOM interferometer and detect when they bunch in the BS. Moving the mirror in one arm of the

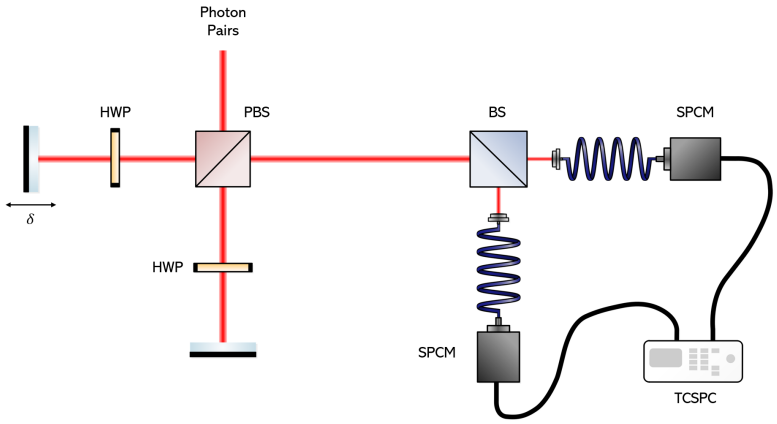

Figure 5.6: Temporal characterization setup.

interferometer creates a path distance difference in one of the photons. To measure the bunching after the BS we mount one SPCM in each resultant arm and connect them to a TCSPC. The TCSPC will register the time difference that each pulse arrives and verify if it is under the coincidence window of 40 ps. The coincidences are detected when each photon of the pair goes through a different path after the BS. If there is photon bunching, the TCSPC does registers much less coincidences. Figure 5.7 shows a graph of the number of coincidences in function of the delay imposed by the mirror in the interferometer. We see that when the mirror is placed such that the photons become indistinguishable in time, the number of coincidences drops significantly (HOM dip). The temporal walk-off is considered negligible when it is very small compared to the coherent length of the photon pairs, which is given by the HOM dip's Full Width at Half Maximum (FWHM).

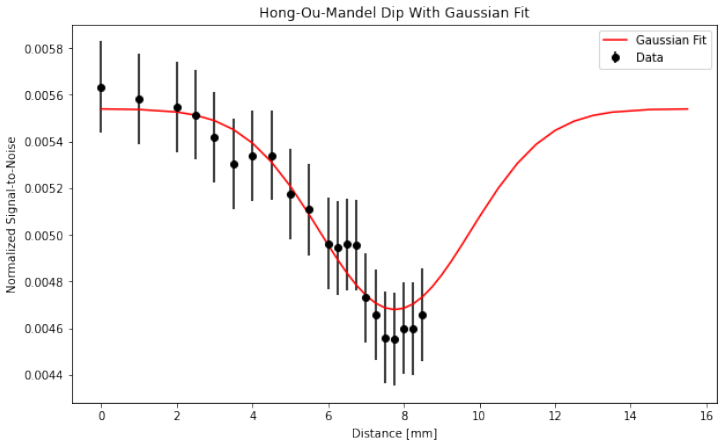

Figure 5.7: Number of coincidences normalized for each position of the movable mirror relative to the fixed mirror.

The HOM dip in Figure 5.7 is fitted with a Gaussian function. The visibility of the HOM dip is given by equation (5.1), where P_c is the coincidence probability and τ is the relative time delay between the

photons arriving at the BS. We measured a visibility of approximately 20 %, and from that determined the coherence length given by the HOM's dip FWHM: 4.72 mm. The visibility obtained is not very high, however it is statistically significant, and sufficient to find a minimum and determine the photon delay between the pairs. One can improve the visibility by introducing a narrower bandpass spectral filter centered around 810 nm. Note that the coherence length measured depends on the coherence length of the laser.

$$V = \frac{P_c\left(\tau \to \infty\right) - P_c\left(\tau = 0\right)}{P_c\left(\tau \to \infty\right)} \tag{5.1}$$

The HOM dip minimum is registered when the mirror is at a distance of 7.75 mm relative to the mirror at the other arm. For a deviation of 7.75 mm the temporal delay is approximately 26 ps. Fixing both mirrors we have compensated the temporal walk-off of the photons outcome state. In the following, the objective is to analyse the correlation of the photon pairs, so we are going to separate them spatially. This will allow us to do the Bell state analysis.

5.4 Entanglement Characterization in The Polarization Degree of Freedom

The characterization of the entanglement comes from the measured visibility of the Bell state analysis. A good visibility (above 71 %, see Appendix B.1) implies the correlation of the photon pairs emitted by the source is capable of violating the CHSH inequality (Bell inequality), which can be seen as an observation of entanglement [47, 48]. The quality of entanglement is thus related to the visibilities obtained. Figure 5.8 shows the experimental setup of the Bell state analysis.

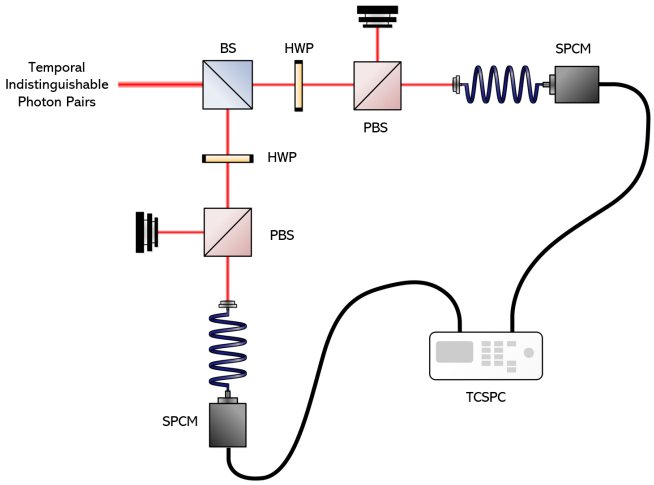

Figure 5.8: Schematic of the Bell state analysis setup.

The generated photon pairs pass through the HOM interferometer, which compensates the temporal delay caused by the nonlinear crystal's birefringence. At the end of each path of the BS, we perform the Bell measurement. The measurement apparatus is composed of a HWP followed by a PBS, on each arm. The projective measurement is executed using the PBSs, which transmit photons with horizontal polarization and reflects photons with vertical polarization. The HWP allows the PBS to analyse the photon's polarization in different directions. Thus we can measure the state (gather coincidence statistics) in a basis of four orthogonal polarization vectors: $\{HV, VH, +-, -+\}$, where $+$ is diagonal polarization $|+\rangle = 1/\sqrt{2}\,(|H\rangle + |V\rangle)$, and $-$ is the antidiagonal polarization $|-\rangle = 1/\sqrt{2}\,(|H\rangle - |V\rangle)$. Indeed, the HWP $+$ PBS measurement system form a new basis obtained by rotation of the horizontal/vertical basis, given by the relation (5.2), where $u = a, b$, are the two possible paths taken by the photons.

$$\begin{pmatrix} |+_u\rangle \\ |-_u\rangle \end{pmatrix} = \begin{pmatrix} -\cos(2\theta_u) & -\sin(2\theta_u) \\ -\sin(2\theta_u) & -\cos(2\theta_u) \end{pmatrix} \begin{pmatrix} |H_u\rangle \\ |V_u\rangle \end{pmatrix} \tag{5.2}$$

In the new basis, the state can now be written as (5.3). This result allows us to measure the photon state on every orthogonal polarization direction by rotating the HWP by a certain angle: 0° for $|HV\rangle$ direction (H basis), 22.5° for $|+-\rangle$ (D basis), 45° for $|VH\rangle$ (V basis), and 67.5° for the $|-+\rangle$ direction (A basis).

$$|\Psi^{\pm}\rangle = \frac{1}{\sqrt{2}}\left[\sin(\theta_a \pm \theta_b)\,|+_a +_b\rangle - \sin(\theta_a \pm \theta_b)\,|-_a -_b\rangle + \cos(\theta_a \pm \theta_b)\,|+_a -_b\rangle + \cos(\theta_a \pm \theta_b)\,|-_a +_b\rangle\right] \tag{5.3}$$

Now it is straightforward to measure the interference fringes in the four polarization directions. One of the HWP remains at a fixed angle, while the other one rotates around a range of 180° to observe the photon pair interference fringes. Note that the reference angle 0° corresponds to the HWP angle which its fast axis is align with the vertical axis (virtual $\hat{y}$ axis). The measurements are shown in Figure 5.9.

The visibilities observed in the data are summarized in Table 5.1. The measurements in the D and A basis show two problems: 1) the points are not exactly at the positions we expect them, measurements in different basis should be translated with respect to each other by a multiple of 22.5° (although in the D basis, we do see some points at the right place), 2) the visibilities are not as high as for the H and V basis. Regarding the second problem, this is expected: the D and A measurements are harder to perform because they are directly related to the entanglement of the state. Measurements on those bases are expected to be more vulnerable to noise [49]. Regarding the first problem, the experiment was done using 10 mW of pump power, which is too high and drastically reduces the entanglement visibility. We have performed numerical simulations for different states of photon pairs, and believe that high visibility in the D and A basis (above 50%) can only be explained by entangled squeezed states with multi-photon components. In other words, we believe we have entanglement, but not the specific

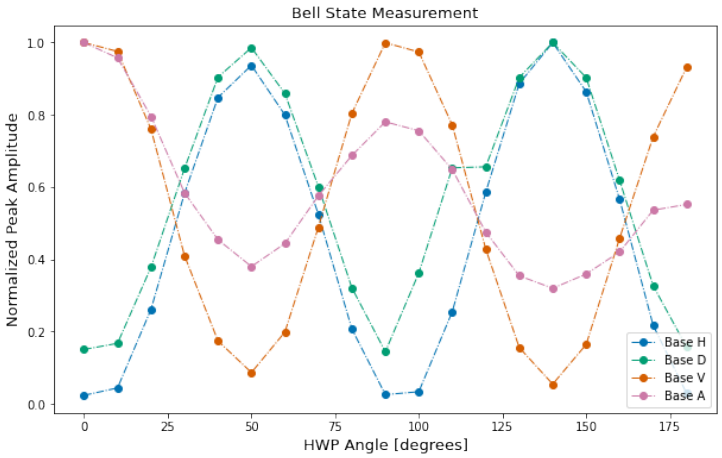

Figure 5.9: Results of the bell state measurement for each basis.

two-qubit entangled state that we want.

Table 5.1: Measured visibilities.

Basis	H	V	D	A
Visibilities	97.65%	94.55%	85.59%	68.02%

6

Application for Quantum Communications

Contents

6.1 BB84 Protocol

The BB84 protocol is one of the most widely used and simple QKD protocols. It has been mathematically proven, that both ends of the communication can detect any attempt to eavesdrop on the key distribution process. The protocol is secure against all classical and quantum attacks [50]. Consider two parties who want to communicate, Alice and Bob in this case. Alice and Bob share two channels, a classical public channel and a quantum communication channel which can transmit qubits. For photons, the channel could be an optical fiber or even free space. The protocol is divided into 7 steps:

1. Alice starts by generating a random string of bits (Key)
2. For each bit, she randomly chooses a base between X and Z to encode into qubit
3. Alice transmits each qubit in order to Bob over a quantum channel
4. Bob randomly chooses a base in which to measure each qubit (X or Z base)
5. Over a classical channel, Bob and Alice share with each other the list of bases they used
6. They discard the bits measured in a different base
7. Alice and Bob now have an identical string of random bits which is called a sifted key

The results measured in a different base compared to the one they were encoded in are discarded because they are unpredictable. Imagine that Alice and Bob choose to use photons as qubits for the communication, in particular the photon's polarization. Alice can encode the key using a horizontal/vertical polarization (Z basis) or using diagonal/anti-diagonal polarization (X basis). If Alice sends a photon with horizontal polarization (a bit valued 0), and Bob measures using X base, in theory, the probability of getting the correct value is 50 %, hence completely random. Otherwise, when Bob chooses the same base, the probability of measuring it correctly is 100 %. Since they choose their basis randomly, only half of the bits sent will not be discarded and result in the sifted key. An example of the protocol is shown in Table 6.1.

Key	0	1	1	0	0	0	1	1
Alice's base	Z	Z	Z	Z	X	X	X	X
Alice's polarization	$\rightarrow$	$\uparrow$	$\uparrow$	$\rightarrow$	$\nearrow$	$\nearrow$	$\searrow$	$\searrow$
Bob's base	Z	X	Z	X	X	Z	Z	X
Bob's measurement	$\rightarrow$	$\nearrow$	$\uparrow$	$\nearrow$	$\nearrow$	$\rightarrow$	$\uparrow$	$\searrow$
Matching basis	✓	×	✓	×	✓	×	×	✓
Sifted key	0		1		0			1

Table 6.1: Example of an implementation of the BB84 protocol. In the end, only half the bits are kept and used to create the sifted key.

The protocol works for sharing a bit key over a quantum channel, thought to understand why BB84 is secure we have to analyse a possible attack. Assuming an eavesdropper, Eve, attacks the communication. If Alice and Bob are secure and perform all the steps perfectly, Eve, can only interfere with the channels of communication (step 3 and 5). The public classical channel is used only to share information about the basis used, so she cannot get access to what Bob actually measured. The only option for Eve is through the information shared over the quantum channel.

For Eve to intercept a qubit in the quantum channel and gather information about its value, she has to measure it. Due to the no-cloning theorem [51], Eve cannot copy and resend the qubit unchanged to Bob. Though, she has to choose a base in which to measure. If she makes a measurement with the same base that Alice encoded, she can resend the qubit to Bob unchanged. However, if the basis are not the same, she has a 50% chance of measuring the correct value. In this case, Eve has changed the Alice's qubit, introducing an error on Bob's side. For example, Alice sends an horizontal polarized photon (Z base), if Eve intercepts it choosing the X basis, she will either measure diagonal or anti-diagonal polarization. This implies Eve sends a diagonal/anti-diagonal photon to Bob. Now, if Bob chooses the same base as Alice, he can measure either horizontal or vertical polarization with 50% chance. As Eve has no more information than Bob, the best option is for her to choose randomly which base to use, then she can alter the qubit half of the times. Bob them starts to have some errors in his measurements. After Alice and Bob share all of the extent of the key, they can check whether Eve intervened by calculating the Bit Error Rate (BER). For this particular attack, Eve introduces a BER of at least $1/4$. However, it is possible to achieve lower BER with more refined attacks [52]. Alice and Bob can defined a threshold for the BER value, in which if the measured BER is higher, the communication is stopped. Imperfections on the physical devices an the quantum channel can also influence the BER value, so its value is chosen in order to maximize the transmission rate while minimizing the information extracted by Eve. Finally, in order to get a secure key, Alice and Bob apply a classical error-correcting algorithms to remedy the effect of random errors caused by noise in the devices.

The protocol requires that Alice is able to generate a single photon and encode one bit of the key in the photon's polarization. Although it is very challenging to build a deterministic single photon source, it is possible to build an apparatus consisting of a photon pair source that can be used as a probabilistic, but heralded, single photon source.

6.2 Portable Quantum Key Distribution

The main objective of this Section is to discuss a design of a specialized portable source that implements QKD protocols (in particular BB84). The goal is to demonstrate the feasibility of the setup which in the future should be miniaturized to fit in a nanosatellite. There are two ways to approach this problem.

The first approach consists in using $810 - 850$ nm light in a free-space configuration. We can use the photon pair source developed in this project as a probabilistic heralded single photon source (HSPS) to send polarization encoded qubits to a receiver. Figure 6.1 show a schematic of our design for the free-space source. In the figure, we show a continuous-wave laser at the source, which is pulsed using a Electro-Optic Amplitude Modulator (EOAM). The information of the key is encoded in the polarization of the light pulses using a Electro-Optic Phase Modulator (EOPM) (see Appendix C.1 for more detailed information). Hence, in the figure, a weak coherent pulse (attenuated light) source is shown. We may also replace the laser and EOAM with a HSPS (Section 6.2.1). In the view of communications with a nanosatellite, this type of single photon source is quite big and hard to miniaturize. For a more compact and (and still secure) solution, one should use weak coherent pulses. Another problem is the bulkiness of the free-space optics, such as the Electro-Optic Modulator (EOM), and the fact that they require high voltages to work properly (furthermore, these high-voltage amplifiers are usually very bulky devices). Therefore, the 850 nm free-space setup is interesting for free-space QKD, but not the most optimized in terms of compactness for nanosatellite communication.

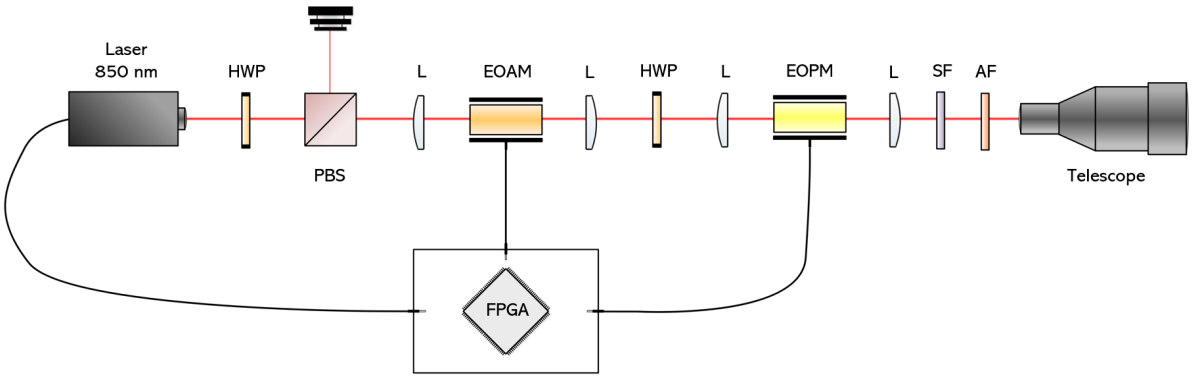

Figure 6.1: Schematic of an heralded single photon source using a photon pair source Schematic of an experimental setup for a free-space QKD emitter. The component L stands for lenses, the component SF stands for Spectral Filter and AF is an Absorption Filter.

The second, much more compact, solution, is to design a fibered system working in a telecom wavelength (1550 nm). Having an all-fibered setup reduces significantly its size. To further reduce the size, we use a weak coherent pulse source instead of a single photon source. These pulses are generated at the emitter, and since they are at the telecom wavelength, they have very good transmission rates through the atmosphere do quantum communication in daylight conditions, because the detectors will in that case be much less sensitive to background light.

6.2.1 Heralded Single Photon Source

BB84 and other types of polarization QKD protocols may use single photon sources for enhanced security. For BB84, Alice needs to generate an individual photon at a time, manipulate its polarization, and then send it to Bob. Unfortunately, single photon sources are not straightforward to produce, in fact, single photon generation is a very hot area of research [53]. Nevertheless, it is possible to use the setup of Chapter 4 to design an HSPS, which we plan to do in the future. These types of sources are not deterministic single photon sources that emit one photon at a time, but rather probabilistic single photon sources, that need photon statistics to ensure similar results. They do have the advantage that they herald the single photon, meaning that when the photon is there, we know it is there. Figure 6.2 shows an illustration of the HSPS apparatus. After generating a beam of photon pairs, the pairs are separated deterministically using a PBS and then right after the separation, one of the pairs is detected using a SPCM.

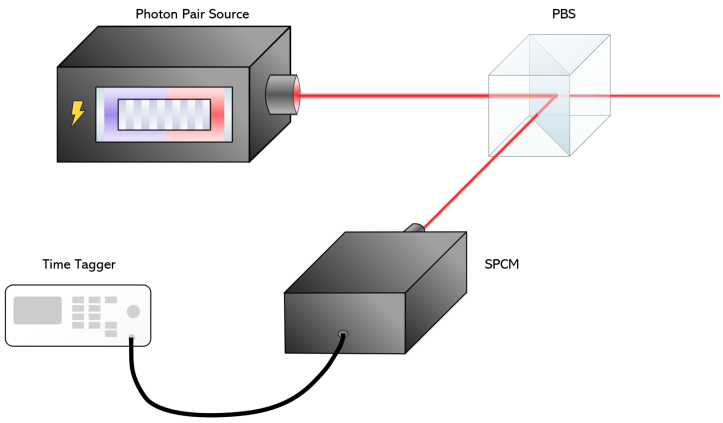

Figure 6.2: Schematic of an heralded single photon source using a photon pair source

For a single photon source to work as desired, it needs to send photons on demand. This means that we should be certain when a single photon is generated. This is achieved by detecting one of the photons of the pair, thereby heralding the presence of the other. In Section 3.1 we saw that in type-II SPDC, each pump photon is converted into a pair of orthogonally polarized photons. So, if they are separated (using a PBS) and we detect one of them, we can say with certainty that there is a photon in the other arm. Since both photons have corrected temporal profiles, Alice can time tag the detected photons at the source and correlate them to the ones that arrived at Bob.

The HSPS setup is harder to miniaturize to fit a 3U CubeSat. In the following, we explore a design for a compact Weak Coherent Pulse (WCP) source which can be built in optical fiber and can be used to implement secure quantum communication.

6.3 Quantum Satellite

QKD is a very promising concept and is proven to achieve, under certain assumptions, unconditionally security. However, in terms of long distance telecommunications, QKD is in an early stage. There are two main approaches to extend QKD to distances of hundreds to thousands of kms: quantum repeaters and space-based QKD.

In this section, we describe a preliminary design of an optical payload for space-based communications with a nanosatellite. This work is part of a project of the Instituto de Telecomunicações called QuantSat-PT, where the goal is to develop an optical payload for a 3U CubeSat. The optical payload consists of a source of quantum states (weak coherent pulses) for three-state one-decoy BB84 inspired from Grünenfelder [54]. The objective is to design a miniaturized version of the setup adapted for a 3U ($10 \times 10 \times 32$ cm^3) CubeSat downlink. CubeSats are cheap miniaturized satellites based around a form factor consisting of 10 cm cube that can be lunched to space as a secondary payload on a launch vehicle (such as the Ariane 6).

6.3.1 Weak Coherent Pulse Source

We can build an experimental setup to test the communication protocol, and to miniaturize it to fit a nanosatellite. In Figure 6.3 is represented a schematic of the experimental setup of the optical emitter (Alice) that will fit in the CubeSat. For this setup we follow the same approach as Grünenfelder [54], with some modifications to make it even more compact. The photons are generated by a telecom laser source (1550 nm). In telecom wavelength, light has a good transmission in free-space, furthermore detectors are not as sensible to visible light which allows for daylight operations. We then use an EOAM to control the intensity of the laser beam and create coherent pulses of light. The width of the pulses depend on the time of activation of the EOAM. Then we need to encode the key information on the photons. For that we use a EOPM to rotate the polarization of the photon to one of three possibilities (see Appendix C.1). As an input for the EOPM, the light should be in an equal superposition of H and V, i.e. $(|H\rangle + |V\rangle)/2$. Since the polarization of the laser photons is unknown, we need to rotate the polarization with a Polarization Controller (PC) before they enter the EOPM. Alice encodes a polarization state by changing the voltage applied on the device. EOMs for telecom wavelength are much faster than for other wavelengths, and consume much less power which is useful for a CubeSat design, and reach higher modulation rates (up to several tens of GHz). Finally, the setup includes a Passive Filter (PF) to attenuate the signal to the right intensity to be sent. Afterwards, the photons are ready to be sent to earth's surface through a telescope.

This experiment is a proof of concept of the emitter. To miniaturize it, we use a fibered setup which makes the setup more compact and consume less energy. The satellite will communicate to a ground

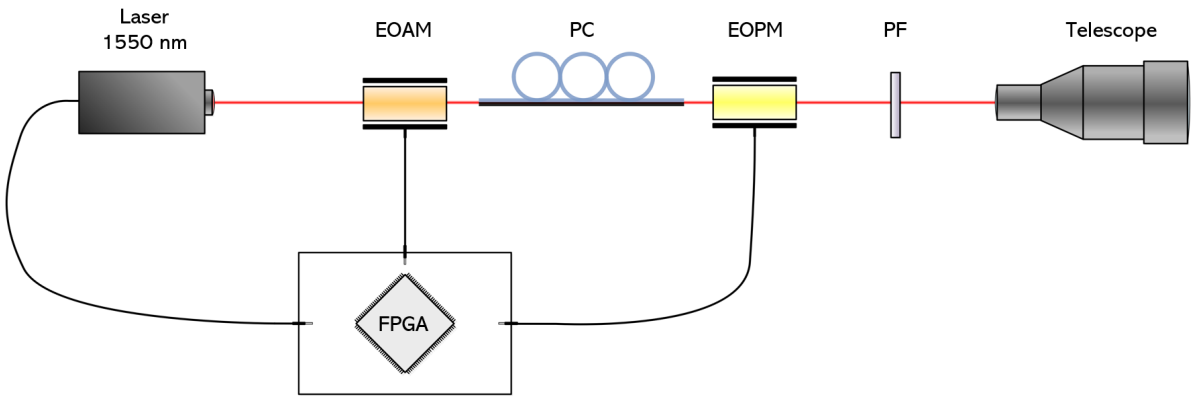

Figure 6.3: Schematic of the experimental setup for quantum satellite

station, that will act as Bob. The ground station capture the photons sent by the satellite using a large telescope, and will perform the quantum measurements. For the communication protocol to work, Bob must choose a random base to measure the photons. A simple way to do that is using a 50-50 BS to split the photons into two paths, and use a different measurement basis in each path. The probability that a photon ends up in one path is exactly 50 %, so the distribution of photons will be completely random. Alice also has to choose a random base to encode information. To this end, the FPGA or a quantum random number generator can be used to generate random numbers.

Finally, the last phase of the protocol is when Alice and Bob share the information of their chosen bases. That can be achieved through communication via a classical channel like radio waves. After that the ground station just needs to run error rate verification algorithms to make sure the security of the channel is not compromised.

6.4 Outlook

Using the schematic presented above, we were able to propose a preliminary design for an optical payload which fits a 3U CubeSat. The design has the advantage of being the most compact design proposed for a CubeSat downlink, and furthermore allows for higher rates, and improved security [54]. The article proposing this design is under preparation, and will be submitted in principle to EPJ Quantum Technology.

7

Conclusion and Outlook

In this thesis, we have built a practical photon pair source for quantum communications. In Chapter 2, we provided a review of the mathematical picture behind quantum information, with an emphasis on quantum correlations, and in Chapter 3 we presented the theory of the nonlinear optical processes used to generate quantum states in our work. In Chapter 4, we present our laboratory implementation of the photon pair source and characterize its output states on Chapter 5. At the end, we present a design of a portable photon source specialized to implement QKD protocols and exploit an application for a nanosatellite.

In Chapter 5 we introduced an easy and cheap alternative to measure the time of arrival of single photons using a FPGA. This allows us to register coincidence events between two SPCM. The FPGA used for the TCSPC is a cheap and easy to use board from Xillinx. The software is very versatile in what concerns programming the circuit, although the timing constraints of the clock's FPGA are very imprecise in the timing scale we are working in. Nevertheless, the concept worked as desired and with a more advanced board it is possible to achieve the timing precision necessary. After these initial experiments, the laboratory acquired a time tagger from Swabian Instruments with state of the art properties. In the future, we would like to have cheap alternatives to TCSPC, to develop cheap and portable quantum communication setups in the lab.

Our source is intended to generate two-qubit quantum states of light, and our results are very promising. During the timeframe of the thesis, we were able to demonstrate the production of correlated photon pairs with orthogonal polarizations, by splitting the polarizations at the output of the crystal and using high-resolution TCSPC. We have measured a brightness of around $45.14\ \frac{\text{kHz}}{\text{mW}}$. In the last phase of the thesis, we were able to start experimenting with the Bell state measurement, which allows to probe the quality of the entangled two-photon pair state. Due to the short time we had, our results pertaining to the Bell state measurement are not yet conclusive, although they are very promising. We have measured a visibility of about $95-97\%$ in the H and V bases, a visibility of close to 86% in the D basis, and a visibility of 68% in the A basis. The D and A basis measurements show a problem: they are in phase with the H and V measurements, respectively. Nevertheless, such high visibilities in the four bases cannot be explained by a classical state of light. In fact, we believe what we did was a Bell state measurement on a squeezed state of light, i.e. with multi-photon pairs. That would explain our results, and makes the solution simple: we need to reduce the pump power. We are at the moment doing this new set of measurements.

Our setup has a few limitations which we are already addressing. Our laser is not very stable, because of the temperature fluctuations and vibrations happening in the building where the laboratory is located. We now have been granted access to a lab in the basement of Torre Norte, and are starting to repeat the measurements. Another limitation is that the spectral filter we used is not very narrow, it is 40 nm wide (FWHM). We have ordered a new, much narrower (10 nm FWHM), spectral filter. This will

improve the visibilities of the HOM and the Bell state measurement.

We also plan to make further improvements in the future: 1) Adding a second PPKTP crystal to directly generate the states we want (instead of post-selecting them like we do), which will lead to better brightness, 2) using a Sagnac loop to improve temporal indistinguishability.

Correlated photon pairs have important applications in quantum communication experiments: entanglement and single photon states (e.g. HSPS) are at the basis of many quantum communication protocols.

The photons generated by the source have a wavelength suited for free space optical communications (810 nm), so in the final Chapter (6) we exploit this property to design a free-space QKD experiment which is already being developed in the lab. The setup will serve as a demonstrator for a QKD state emitter which will be miniaturized in the future to fit inside a 3U CubeSat. The architecture of the satellite is an active design which depends on electronics to generate the random key and control the state encoders (EOM). All this can be controlled with an FPGA which can easily fit in a satellite.

The photon pair source studied in this work has been demonstrated before, but to the extend of my knowledge (and my supervisor's) this is the only quantum entanglement source presently existing in Portugal. We are already working on improving the source, and have ideas for future compact sources, including of more complex quantum states than the ones considered in this thesis. This provides a solid basis for further work on the laboratory in developing highly efficient, fiber-compatible sources for quantum communication networks. Furthermore, these sources are important to study materials, for example for optical quantum memory applications. Hence, we expect this source may also lead to new projects arising from collaborations with other groups in and outside Instituto Superior Técnico.

Bibliography

[1] R. W. Boyd, *Nonlinear Optics*. New York: Academic Press, 1992.

[2] A. Einstein, B. Podolsky, and N. Rosen, "Can quantum-mechanical description of physical reality be considered complete?" *Phys. Rev.*, vol. 47, pp. 777–780, May 1935.

[3] J. S. Bell, "On the einstein podolsky rosen paradox," *Physics Physique Fizika*, vol. 1, pp. 195–200, Nov 1964.

[4] A. Aspect, P. Grangier, and G. Roger, "Experimental realization of einstein-podolsky-rosen-bohm gedankenexperiment: A new violation of bell's inequalities," *Phys. Rev. Lett.*, vol. 49, pp. 91–94, Jul 1982.

[5] M. Nielsen, *Quantum Computation and Quantum Information*. Cambridge: Cambridge University Press, 2010.

[6] J. L. O'Brien, "Optical quantum computing," *Science*, vol. 318, no. 5856, pp. 1567–1570, Dec 2007.

[7] S. Pirandola, B. Bardhan, T. Gehring, and *et al.*, "Advances in photonic quantum sensing," *Nature Photon*, vol. 12, pp. 724–733, Nov 2018.

[8] N. Gisin and R. Thew, "Quantum communication," *Nature Photon*, vol. 1, pp. 165–171, Mar 2007.

[9] C. Bennett and G. Brassard, "Quantum cryptography: Public key distribution and coin tossing," *Proceedings of the International Conference on Computers, Systems & Signal Processing*, pp. 175–179, Dec 1984.

[10] A. K. Ekert, "Quantum cryptography based on bell's theorem," *Physical Review Letters*, vol. 67, pp. 661–663, Aug 1991.

[11] C. H. Bennett, G. Brassard, C. Crépeau, R. Jozsa, A. Peres, and W. K. Wootters, "Teleporting an unknown quantum state via dual classical and einstein-podolsky-rosen channels," *Phys. Rev. Lett.*, vol. 70, pp. 1895–1899, Mar 1993.

[12] D. Bouwmeester, J.-W. Pan, K. Mattle, M. Eibl, H. Weinfurter, and A. Zeilinger, “Experimental quantum teleportation,” *Nature*, vol. 390, pp. 575–579, Dec 1997.

[13] S. Takeuchi, “Recent progress in single-photon and entangled-photon generation and applications,” *Japanese Journal of Applied Physics*, vol. 53, no. 3, p. 030101, Feb 2014.

[14] K. Mattle, H. Weinfurter, P. G. Kwiat, and A. Zeilinger, “Dense coding in experimental quantum communication,” *Phys. Rev. Lett.*, vol. 76, pp. 4656–4659, Jun 1996.

[15] M. Krenn, M. Malik, T. Scheidl, R. Ursin, and A. Zeilinger, “Quantum communication with photons,” *Optics in our Time*, vol. 18, p. 455, Dec 2016.

[16] J. Yin, Y. Li, S. Liao, and *et al.*, “Entanglement-based secure quantum cryptography over 1,120 kilometres,” *Nature*, vol. 582, pp. 501–505, Jun 2020.

[17] I. L. Chuang and Y. Yamamoto, “Simple quantum computer,” *Phys. Rev. A*, vol. 52, pp. 3489–3496, Nov 1995.

[18] S. Shi, B. Xu, K. Zhang, and *et al.*, “High-fidelity photonic quantum logic gate based on near-optimal rydberg single-photon source,” *Nature Communications*, vol. 13, p. 4454, Aug 2022.

[19] I. Georgescu, “25 years of experimental quantum teleportation,” *Nat Rev Phys*, Oct 2022.

[20] F. Schlawin, K. E. Dorfman, and S. Mukamel, “Entangled two-photon absorption spectroscopy,” *Accounts of chemical research*, vol. 51, no. 9, pp. 2207–2214, Sep 2018.

[21] M. B. Nasr, A. F. Abouraddy, M. C. Booth, B. E. A. Saleh, A. V. Sergienko, M. C. Teich, M. Kempe, and R. Wolleschensky, “Biphoton focusing for two-photon excitation,” *Phys. Rev. A*, vol. 65, p. 023816, Jan 2002.

[22] S. M. Lee, H. Kim, M. Cha, and H. S. Moon, “Polarization-entangled photon-pair source obtained via type-ii non-collinear spdc process with ppktp crystal,” *Optics express*, vol. 24, no. 3, pp. 2941–2953, Feb 2016.

[23] O. Cohen, J. S. Lundeen, B. J. Smith, G. Puentes, P. J. Mosley, and I. A. Walmsley, “Tailored photon-pair generation in optical fibers,” *Phys. Rev. Lett.*, vol. 102, p. 123603, Mar 2009.

[24] C. Couteau, “Spontaneous parametric down-conversion,” *Contemporary Physics*, vol. 59, no. 3, pp. 291–304, Jun 2018.

[25] Y. Shih, “Entangled biphoton source - property and preparation,” *Reports on Progress in Physics*, vol. 66, no. 6, pp. 1009–1044, may 2003.

[26] M. P. Silverman, *A certain uncertainty: nature’s random ways*. Cambridge University Press, 2014.

[27] E. Diamanti, H. Lo, B. Qi, and *et al.*, "Practical challenges in quantum key distribution," *npj Quantum Information*, vol. 2, p. 16025, Nov 2016.

[28] E. Gibney, "One giant step for quantum internet," *Nature*, vol. 535, no. 7613, pp. 478–479, Jun 2016.

[29] J.-G. Ren, P. Xu, H.-L. Yong, L. Zhang, S.-K. Liao, J. Yin, W.-Y. Liu, W.-Q. Cai, M. Yang, L. Li *et al.*, "Ground-to-satellite quantum teleportation," *Nature*, vol. 549, no. 7670, pp. 70–73, Aug 2017.

[30] S.-K. Liao, W.-Q. Cai, W.-Y. Liu, L. Zhang, Y. Li, J.-G. Ren, J. Yin, Q. Shen, Y. Cao, Z.-P. Li *et al.*, "Satellite-to-ground quantum key distribution," *Nature*, vol. 549, no. 7670, pp. 43–47, Aug 2017.

[31] H. Takenaka, A. Carrasco-Casado, M. Fujiwara, M. Kitamura, M. Sasaki, and M. Toyoshima, "Satellite-to-ground quantum-limited communication using a 50-kg-class microsatellite," *Nature photonics*, vol. 11, no. 8, pp. 502–508, Jul 2017.

[32] T. Jennewein, J. P. Bourgoin, B. Higgins, C. Holloway, E. Meyer-Scott, C. Erven, B. Heim, Z. Yan, H. Hübel, G. Weihs, E. Choi, I. D'Souza, D. Hudson, and R. Laflamme, "QEYSSAT: a mission proposal for a quantum receiver in space," *Advances in Photonics of Quantum Computing, Memory, and Communication VII*, vol. 8997, p. 89970A, Feb 2014.

[33] E. Kerstel, A. Gardelein, M. Barthelemy, M. Fink, S. K. Joshi, and R. Ursin, "Nanobob: a cubesat mission concept for quantum communication experiments in an uplink configuration," *EPJ Quantum Technology*, vol. 5, no. 1, p. 6, Jun 2018.

[34] C. Agnesi, F. Vedovato, M. Schiavon, D. Dequal, L. Calderaro, M. Tomasin, D. G. Marangon, A. Stanco, V. Luceri, G. Bianco *et al.*, "Exploring the boundaries of quantum mechanics: advances in satellite quantum communications," *Philosophical Transactions of the Royal Society A: Mathematical, Physical and Engineering Sciences*, vol. 376, no. 2123, p. 20170461, may 2018.

[35] D. K. L. Oi, A. Ling, J. A. Grieve, T. Jennewein, A. N. Dinkelaker, and M. Krutzik, "Nanosatellites for quantum science and technology," *Contemporary Physics*, vol. 58, no. 1, pp. 25–52, Nov 2017.

[36] W. Zhang, T. van Leent, K. Redeker, and *et al.*, "A device-independent quantum key distribution system for distant users," *Nature*, vol. 607, pp. 687–691, Jul 2022.

[37] J. F. Clauser, M. A. Horne, A. Shimony, and R. A. Holt, "Proposed experiment to test local hidden-variable theories," *Phys. Rev. Lett.*, vol. 23, pp. 880–884, Oct 1969.

[38] M.-X. Luo, H.-R. Li, H. Lai, and X. Wuang, "Quantum computation based on photons with three degrees of freedom," *Scientific Report*, vol. 6, p. 25977, May 2016.

[39] R. Loudon, *Quantum Computation and Quantum Information*. Oxford: Oxford University Press, 2000.

[40] P. Sekatski, N. Sangouard, F. Bussières, C. Clausen, N. Gisin, and H. Zbinden, "Detector imperfections in photon-pair source characterization," *Journal of Physics B: Atomic, Molecular and Optical Physics*, vol. 45, p. 124016, Jun 2012.

[41] J. A. Armstrong, N. Bloembergen, J. Ducuing, and P. S. Pershan, "Interactions between light waves in a nonlinear dielectric," *Phys. Rev.*, vol. 127, pp. 1918–1939, Sep 1962.

[42] P. G. Kwiat, E. Waks, A. G. White, I. Appelbaum, and P. H. Eberhard, "Ultrabright source of polarization-entangled photons," *Phys. Rev. A*, vol. 60, pp. R773–R776, Aug 1999.

[43] M. A. Golub, S. V. Karpeev, K. S. G., A. M. Prokhorov, I. N. Sisakyan, and V. A. Soĭfer, "Spatial filter investigation of the distribution of power between transverse modes in a fiber waveguide," *Soviet Journal of Quantum Electronics*, vol. 14, no. 9, p. 1255, sep 1984.

[44] H. Lee, H. Kim, M. Cha, and *et al.*, "Simultaneous type-0 and type-ii spontaneous parametric down-conversions in a single periodically poled ktiopo$_4$ crystal," *Applied Physics B*, vol. 108, pp. 585–589, Jun 2012.

[45] J. Park, T. Jeong, H. Kim, and H. S. Moon, "Time-energy entangled photon pairs from doppler-broadened atomic ensemble via collective two-photon coherence," *Phys. Rev. Lett.*, vol. 121, p. 263601, Dec 2018.

[46] C. K. Hong, Z. Y. Ou, and L. Mandel, "Measurement of subpicosecond time intervals between two photons by interference," *Phys. Rev. Lett.*, vol. 59, pp. 2044–2046, Nov 1987.

[47] R. Horodecki, P. Horodecki, M. Horodecki, and K. Horodecki, "Quantum entanglement," *Rev. Mod. Phys.*, vol. 81, pp. 865–942, Jun 2009.

[48] K. Bartkiewicz, B. Horst, K. Lemr, and A. Miranowicz, "Entanglement estimation from bell inequality violation," *Phys. Rev. A*, vol. 88, p. 052105, Nov 2013.

[49] M. Jabir and G. Samanta, "Robust, high brightness, degenerate entangled photon source at room temperature," *Scientific reports*, vol. 7, no. 1, pp. 1–8, 2017.

[50] P. W. Shor and J. Preskill, "Simple proof of security of the bb84 quantum key distribution protocol," *Phys. Rev. Lett.*, vol. 85, pp. 441–444, Jul 2000.

[51] W. Wootters and W. Zurek, "A single quantum cannot be cloned," *Nature*, vol. 299, pp. 802–803, Oct 1982.

[52] D. Bruß, M. Cinchetti, G. Mauro D'Ariano, and C. Macchiavello, "Phase-covariant quantum cloning," *Phys. Rev. A*, vol. 62, p. 012302, Jun 2000.

[53] S. Scheel, "Single-photon sources–an introduction," *Journal of Modern Optics*, vol. 56, no. 2-3, pp. 141–160, Oct 2009.

[54] F. Grünenfelder, A. Boaron, D. Rusca, A. Martin, and H. Zbinden, "Simple and high-speed polarization-based qkd," *Applied Physics Letters*, vol. 112, no. 5, p. 051108, Jan 2018.

[55] J. D. Bierlein and H. Vanherzeele, "Potassium titanyl phosphate: properties and new applications," *JOSA B*, vol. 6, no. 4, pp. 622–633, May 1989.

[56] S. Emanueli and A. Arie, "Temperature-dependent dispersion equations for ktiopo4 and ktioaso4," *Appl. Opt.*, vol. 42, pp. 6661–6665, Nov 2003.

[57] F. Consoli, R. De Angelis, L. Duvillaret, and *et al.*, "Time-resolved absolute measurements by electro-optic effect of giant electromagnetic pulses due to laser-plasma interaction in nanosecond regime," *Scientific Reports*, vol. 6, no. 1, p. 27889, Jun 2016.

[58] T. Robinson, F. Consoli, S. Giltrap, S. Eardley, and *et al.*, "Low-noise time-resolved optical sensing of electromagnetic pulses from petawatt laser-matter interactions," *Scientific Reports*, vol. 7, no. 1, pp. 1–12, Apr 2017.

Appendix A

A.1 PPKTP Crystal's Refractive Index

The crystal's refractive index not only differs with the direction x, y, z but also varies with the temperature of the crystal. To model the refractive index for the pump and idler photons (polarized in the z-direction) and the signal photon (polarized in the y-direction) is used the Sellmeier equation [55] which is given by (A.1).

$$n_{y,z}(\lambda, T) = \sqrt{A + \frac{B}{1 - C/\lambda^2} - D\lambda^2} + \Delta n_{y,z}(\lambda, T) \tag{A.1}$$

Where λ is the wavelength of the photon in μm, T is the temperature of the crystal and A,B,C and D are constants for a PPKTP found in Table A.1. The term $\Delta n_{y,z}(\lambda, T)$ is a temperature correction for the Sellmeier equation [56] given by the expressions (A.2).

$$\Delta n_{y,z}(\lambda, T) = n_1(\lambda)(T - T_0) + n_2(\lambda)(T - T_0)^2$$
$$n_{1,2}(\lambda) = \sum_{m=0}^{3} \frac{a_m}{\lambda^m} \tag{A.2}$$

Where T_0 is the temperature of the laboratory and a_m are also constants for a PPKTP found in Table A.2. This way is possible to control the photon pair's emission angle by tunning the crystal's temperature with an electric oven.

Table A.1: Sellmeier Constants

Constant	Value for n_y	Value for n_z
A	2.1518	2.3136
B	0.87862	1.00012
C $[\mu m^2]$	0.21801	0.23831
D $[\mu m^{-2}]$	0.01327	0.01679

Table A.2: Sellmeier Correction Constants

	Value for Δn_y		Value for Δn_z	
a_m	$n_1[10^{-6}]$	$n_2[10^{-8}]$	$n_1[10^{-6}]$	$n_2[10^{-8}]$
a_0	6.2897	-0.14445	9.9587	-1.1882
a_1	6.3061	2.2244	9.9228	10.459
a_2	-6.0629	-3.5770	-8.9603	-9.8136
a_3	2.6486	1.3470	4.1010	3.1481

A.2 SPDC: Signal's and Idler's Emission Angles

The mismatch equation (3.13) needs to be zero for verifying the PM conditions. Because of this, the signal and idler propagation directions depend on the wavevector magnitudes. Assuming that the incident light beam (pump) is parallel to the optical axis of the crystal. The pump wavevector has the same direction as the grating wavevector. So the mismatch vector can be analyzed in its two components, a parallel to the optical axis $\Delta\vec{k}_{\parallel} = 0$ and a perpendicular one $\Delta\vec{k}_{\perp} = 0$, given by (A.3).

$$\begin{aligned} \Delta\vec{k}_{\parallel} &= k_p - k_s\cos(\theta_s) - k_i\cos(\theta_i) - k_g \\ \Delta\vec{k}_{\perp} &= k_s\sin(\theta_s) - k_i\sin(\theta_i) \end{aligned} \tag{A.3}$$

The magnitude of the wave vectors are $|\vec{k_j}| = \frac{2\pi c}{\lambda_j} n_j$ where $j = p, s, i$, λ_j and n_j are the wavelenghts and the refractive indices, respectively. The refractive index depend on the light polarization because of the birefringence of the crystal. With the second equation of (A.3) and respective wavevectors magnitudes, the idler's direction θ_i can be written as a function of the signal's direction θ_s (A.4).

$$\theta_i = \arcsin\left(\frac{n_s\lambda_i}{n_i\lambda_s}\sin\theta_s\right) \tag{A.4}$$

The direction of the idler photon propagation depends on the frequencies, respective refractive indices, and the direction of the signal photon. For the parallel component, the pump wave-vector $\vec{k}_p$

and the grating wave-vector $\vec{k}_g$ also contribute. Again, taking the PM conditions and relation (A.4), the expression for the direction of propagation of the signal photon becomes (A.5) after some algebra.

$$\theta_s \approx \pm \sqrt{\frac{2n_i\lambda_s}{n_s\lambda_i}\left[1 + \frac{\Lambda^{-1} - \frac{n_p}{\lambda_p}}{\frac{n_s}{\lambda_s} + \frac{n_i}{\lambda_i}}\right]} \tag{A.5}$$

Expanding this result to three dimensions, the two symmetrical solutions in the equation imply that the photon pairs' spatial profile has a ring shape. The propagation of the signal photon depends on the wavelengths of the pump and the photon pairs (that must obey the energy conservation law (3.13)), and the properties of the crystal itself, such as the refractive indices n_j and the period of the grating structure Λ. Finally, the signal and idler emission angles at the exit of the crystal are determined by applying Snell's law.

B

Appendix B

B.1 Bell State Analyser

The Bell state analysis done in this section follows the same approach as []. Suppose two qubits A and B encoded in polarization. Each qubit has a two-dimensional Hilbert space, with an orthonormal basis $\{|H_Q\rangle, |V_Q\rangle\}$, with $Q = A, B$. If both qubits compose an entangled system, the orthonormal basis for the new Hilbert space is composed by the four bell states (B.1, B.2), where $\theta = \{0, \pi\}$.

$$|\Phi^{\phi}\rangle = \frac{1}{\sqrt{2}}\left[|H_A, H_B\rangle + e^{i\phi}|V_A, V_B\rangle\right] \tag{B.1}$$

$$|\Psi^{\phi}\rangle = \frac{1}{\sqrt{2}}\left[|H_A, V_B\rangle + e^{i\phi}|V_A, H_B\rangle\right] \tag{B.2}$$

The state to be measured at the PBS is derivated after acting the HWP operator $\hat{U}_{HWP}$ (eq. B.4), over the bell state of the biphoton system. The probability of measuring the state in the base $|H_A, H_B\rangle$ is given by equation B.3, where we projected the state onto the base and calculate the square norm. To compute other basis ($|V_A, V_B\rangle$, $|H_A, V_B\rangle$ and $|V_A, H_B\rangle$) is just project the state onto the respective base.

$$P^{\phi}_{HH}(\theta_1,\theta_2) = ||\langle H_A, H_B|\hat{U}_{HWP}(\theta_1,\theta_2)|\Psi^{\phi}\rangle||^2 = -\frac{1}{\sqrt{2}}\left[\cos 2\theta_1 \cos 2\theta_2 - e^{i\phi}\sin 2\theta_1 \sin 2\theta_2\right] \tag{B.3}$$

$$\hat{U}_{HWP}(\theta_1,\theta_2) = \begin{pmatrix} -i\cos 2\theta_1 & -i\sin 2\theta_1 \\ -i\sin 2\theta_1 & i\cos 2\theta_1 \end{pmatrix}_A \otimes \begin{pmatrix} -i\cos 2\theta_2 & -i\sin 2\theta_2 \\ -i\sin 2\theta_2 & i\cos 2\theta_2 \end{pmatrix}_B \tag{B.4}$$

Now, we can compute the expected value , $E^{\phi}(\theta_1,\theta_2) = P^{\phi}_{HH}(\theta_1,\theta_2) + P^{\phi}_{VV}(\theta_1,\theta_2) - P^{\phi}_{HV}(\theta_1,\theta_2) - P^{\phi}_{VH}(\theta_1,\theta_2)$, and with this result we can calculate the Bell parameter S^{ϕ} using the equation (B.5).

$$\begin{aligned} S^{\phi}(\theta_1,\theta_2,\theta_1',\theta_2') &= E^{\phi}(\theta_1,\theta_2) + E^{\phi}(\theta_1',\theta_2) + E^{\phi}(\theta_1,\theta_2') - E^{\phi}(\theta_1',\theta_2') \\ &= \cos^2\left(\frac{\phi}{2}\right)\left[\cos 2(\theta_1-\theta_2) + \cos 2(\theta_1'-\theta_2) + \cos 2(\theta_1-\theta_2') - \cos 2(\theta_1'-\theta_2')\right] \\ &+ \sin^2\left(\frac{\phi}{2}\right)\left[\cos 2(\theta_1+\theta_2) + \cos 2(\theta_1'+\theta_2) + \cos 2(\theta_1+\theta_2') - \cos 2(\theta_1'+\theta_2')\right] \end{aligned} \tag{B.5}$$

Here the letters θ_1 and θ_2 are the angles of the HWPs where the qubit A and B are measured has $|0\rangle$, respectively. The counterparts θ_1' and θ_2' are measurements on the qubits that yield $|1\rangle$. Computing the partial derivatives of the bell parameter and finding its zeros, is straightforward to find it's maximum value (B.6).

$$S^{\phi}_{max} = 2\sqrt{\cos^2(\phi)+1} \tag{B.6}$$

One can easily verify that for the values 0 and π of the phase ϕ lead to a maximal violation of the Bell inequalities, $S_{max} = 2\sqrt{2}$. For all other values of ϕ the Bell inequality is verified and, therefore, there is no violation (no entanglement). However it is possible to generalize this formalism such that the Bell inequality is violated for all values of ϕ.

C

Appendix C

C.1 Electro-Optic Modulator

After generating single photons with a source, Alice needs to encode the key's information in their polarization. For that, it is necessary an EOM to modulate the polarization of the photons. The EOM is an optical device composed with a material whose optical properties change in response to an slowly variable electric field (slowly compared to the light's frequency), it may modulate the phase, frequency, amplitude or polarization of the light beam. This device can be automated connecting it to a microcontroller chip, such as a computer or a FPGA.

The simplest type of EOM is a phase modulating EOM made of a crystal, such as lithium niobate ($LiNbO_3$), whose refractive index if a function of the strength of the electric field. When the crystal is exposed to an electric field, light will travel through it more slowly. this will cause a phase change at the exit of the crystal proportional to the length of time it takes to pass through the crystal. The voltage required for inducing a phase change of π is called the half-wave voltage V_π, which can go up to hundreds of volts for some EOMs. So, to control this devices it is necessary to connect the microcontroller to a high-voltage amplifier. Also, a phase modulating EOM can be used as an EOAM by using a Mach-

Zehnder interferometer. The objective of this alternative technique is to separate the beam into two paths, each one with a phase modulating EOM introducing an individual phase to each beam. Then, the beams are recombined and can interfere constructively or destructively at the exit. Changing the electric field applied at each path, it is possible ton control the interference and therefore, the intensity of the exiting light.

The Polarization encoding is done by a polarization modulator, such as a titanium indiffused $LiNbO_3$ EOPM. The device modulates the relative phase ϕ between $|H\rangle$ and $|V\rangle$ by inducing an electric field on the crystal to change its birefringence. The light pulses enter with a polarization state of $(|H\rangle + |V\rangle)/2$, and at the exit their state becomes $(|H\rangle + e^{i\phi}|V\rangle)/2$.. Due to the birefringence of the crystal, the EOPM introduces a polarization mode delay. Polarization modulators in elector-optic crystals are used as a technique for time-resolved measurements of unknown electric fields in plasmas [57, 58].